

## Subpolar Southern Ocean Response to Changes in the Surface Momentum, Heat, and Freshwater Fluxes under 2xCO<sub>2</sub>

FABIO BOEIRA DIAS,<sup>a,b,c</sup> CATIA M. DOMINGUES,<sup>a,c,d</sup> SIMON J. MARSLAND,<sup>a,b,c</sup> STEPHEN R. RINTOUL,<sup>e,f,g</sup> PETTERI UOTILA,<sup>h</sup> RUSSELL FIEDLER,<sup>e</sup> MAURICIO M. MATA,<sup>i</sup> NATHANIEL L. BINDOFF,<sup>a,c</sup> AND ABHISHEK SAVITA,<sup>a,b,c</sup>

<sup>a</sup> *Institute for Marine and Antarctic Studies, University of Tasmania, Hobart, Tasmania, Australia*

<sup>b</sup> *CSIRO Oceans and Atmosphere, Aspendale, Victoria, Australia*

<sup>c</sup> *ARC Centre of Excellence for Climate Extremes, University of Tasmania, Hobart, Tasmania, Australia*

<sup>d</sup> *National Oceanographic Centre, Southampton, United Kingdom*

<sup>e</sup> *CSIRO Oceans and Atmosphere, Hobart, Tasmania, Australia*

<sup>f</sup> *Centre for Southern Hemisphere Oceans Research, Hobart, Tasmania, Australia*

<sup>g</sup> *Australian Antarctic Program Partnership, Hobart, Tasmania, Australia*

<sup>h</sup> *Institute for Atmospheric and Earth Science Research, University of Helsinki, Helsinki, Finland*

<sup>i</sup> *Instituto de Oceanografia, Universidade Federal do Rio Grande, Rio Grande, Brazil*

(Manuscript received 25 February 2021, in final form 9 August 2021)

**ABSTRACT:** The Antarctic subpolar Southern Ocean (sSO) has fundamental climate importance. Antarctic Bottom Water (AABW) originates in the sSO and supplies the lower limb of the meridional overturning circulation (MOC), occupying 36% of ocean volume. Climate models struggle to represent continental shelf processes that form AABW. We explore sources of persistent model biases by examining response of the sSO to perturbations in surface forcing in a global ocean–sea ice model (ACCESS-OM2) that forms AABW both on shelf and in open ocean. The sSO response to individual and combined perturbations of surface heat, freshwater, and momentum fluxes follows the WCRP CMIP6 FAFMIP-protocol. Wind perturbation (i.e., a poleward shift and intensification of the westerlies) is dominant, enhancing AABW formation and accelerating the global MOC. This occurs through upwelling of warm waters and inhibition of sea ice growth during winter, which triggers large open water polynya (OWP) events with associated deep convection. These events occur in the Weddell and Ross Seas and their variability is associated with availability of heat at midocean depths. These OWPs cease when the heat reservoir is depleted. Effects of surface warming and freshening only partially compensate changes from increasing winds on ocean stratification and depletion of AABW formation. These results indicate that overly convective models, such ACCESS-OM2, can respond to CO<sub>2</sub>-perturbed scenarios by forming too much AABW in OWP, which might not hold in models without OWPs. This might contribute to the large intermodel spread thermosteric sea level projections, being relevant to the interpretation of future projections by current climate models.

**KEYWORDS:** Abyssal circulation; Deep convection; Meridional overturning circulation; Ocean circulation; Climate models; Climate variability


### 1. Introduction

The global meridional overturning circulation (MOC) has a fundamental role with regard to Earth's climate. It transports heat, salt, and other tracers (e.g., nutrients, oxygen, carbon) around the ocean through different branches (Kuhlbrodt et al. 2007): poleward transport of light waters by surface currents, the formation and sinking of dense waters at high latitudes to the deep ocean and their subsequent equatorward transport by deep

currents, and the eventual upwelling from depth to toward the ocean surface.

The densest water mass of the global ocean, the Antarctic Bottom Water (AABW), originates at the Antarctic continental shelf, sinks down the continental slope and is transported northward as the lower limb of the MOC, filling approximately 36% of the global ocean volume (Johnson 2008). The AABW is formed via mixing between Circumpolar Deep Waters (CDW) that upwell around Antarctica (as part of the MOC) and Antarctic shelf waters (Orsi et al. 1999), including High Salinity Shelf Water (HSSW, a product of sea ice formation), Winter Water (WW), and Ice Shelf Water (ISW) (e.g., Baines and Condie 1985; Rintoul 2007; Ohshima et al. 2013).

The observed changes in AABW during past decades indicate warming and/or freshening of bottom water properties with corresponding decreases in density (e.g., Rintoul 2007; Kerr et al. 2009; Purkey and Johnson 2010, 2013; Fahrbach et al. 2011; Durack et al. 2014). However, more recent studies reveal that these trends could be a slowing or even changing sign in recent years (Abrahamsen et al. 2019; Silvano et al. 2020; Aoki

 Denotes content that is immediately available upon publication as open access.

Fabio Boeira Dias' current affiliation: Institute for Atmospheric and Earth Science Research, University of Helsinki, Helsinki, Finland.

*Corresponding author:* Fabio Boeira Dias, fabio.boeiradias@helsinki.fi

DOI: 10.1175/JCLI-D-21-0161.1

© 2021 American Meteorological Society. For information regarding reuse of this content and general copyright information, consult the [AMS Copyright Policy \(www.ametsoc.org/PUBSReuseLicenses\)](#).

et al. 2020), and that these trends are actually part of natural decadal variability (Zhang et al. 2019). Based on satellite observations, interannual variability of sea ice production in various coastal polynyas (a proxy for dense shelf water formation, a precursor of AABW) has shown a mixed signal, with positive trends in some polynyas (e.g., the Barrier and the Amundsen and Bellingshausen polynyas) and negative trends in others (e.g., Cape Darnley, Mertz Glacier) (Tamura et al. 2016), and some with nonsignificant trends (e.g., the Ross Sea) (Comiso et al. 2011; Drucker et al. 2011). A coupled sea ice–ocean model with sufficient resolution to resolve coastal polynyas ( $\sim 10$  km) indicates that surface warming and increased precipitation reduce the generation and export of dense shelf waters (Marsland et al. 2007).

While AABW changes during the historical period are not necessarily the same as in future scenarios, idealized  $\text{CO}_2$ -increased simulations from climate models can provide insights into the role of surface forcing for long-term changes in the subtropical Southern Ocean (south of  $60^\circ\text{S}$ , hereafter referred to as sSO). In general, climate model simulations under  $\text{CO}_2$ -increased scenarios indicate decline of high-latitude convection (Gregory 2000; Palter et al. 2013). In the sSO, the surface freshwater input is expected to increase the upper-ocean stratification and reduce convection (de Lavergne et al. 2014), while changes in the westerlies (strengthening and poleward shift) have been associated with increase of convection (Frankcombe et al. 2013; Kuhlbrodt et al. 2015). The latest results from the Flux-Anomaly-Forced Model Intercomparison Project (FAFMIP) reinforces this view that the individual contributions from the different surface flux components cause the depth-integrated ocean heat content (OHC) in the sSO to increase under heat and freshwater perturbations and to largely decrease due to increased in the momentum (wind stress) fluxes (Gregory et al. 2016; Couldrey et al. 2021).

The sSO is expected to contribute to sea level rise through thermal expansion (Church et al. 2011; Purkey and Johnson 2013) and mass loss from the Antarctic Ice Sheet (Naughten et al. 2018; Oppenheimer et al. 2019)—the largest contributors to global mean sea level budget (Church et al. 2013). While the land-ice contribution is just starting to be accounted in climate projections (Nowicki et al. 2016), the thermosteric effect (associated with ocean heat uptake and thermal expansion) on the dynamic sea level (i.e., changes in sea surface height relative to the geoid, determined by ocean dynamics and density) has for a long time been considered in climate projections. Current sea level projections, however, exhibit large regional uncertainties that have been linked with the ocean response to a warming climate and the vertical heat transport efficiency (Kuhlbrodt and Gregory 2012; Gregory et al. 2016; Couldrey et al. 2021). The FAFMIP experiments aim to better understand the spread in sea level projections by forcing different climate models with identical surface flux perturbations of heat, freshwater, and momentum, isolating the ocean's response to each. Here, we investigate how sSO heat transport and watermass properties respond to FAFMIP perturbations (representative of a  $2\times\text{CO}_2$  scenario) to gain new process-based insights into the likely causes of discrepancies among models themselves and also with observed trends.

One hypothesis for the discrepancies between long-term sSO trends in models and observations might arise due to the poor representation of AABW formation in coarse ocean and coupled climate models, where bottom water is formed by deep convection in open water polynyas (OWPs) rather than on the Antarctic continental shelf (Heuzé et al. 2015; Aguiar et al. 2017; Mohrmann et al. 2021). Large OWPs are rarely observed in reality, with small OWPs often observed in the twentieth century (Comiso and Gordon 1987; Tamura et al. 2011). Notably, a large OWP ( $250\,000\text{ km}^2$ ) was first observed in the Weddell Sea in the mid-1970s (Zwally and Gloersen 1977; Carsey 1980), and again in 2018, but with a size about one-third of the 1970s polynya (Campbell et al. 2019). Previous studies suggested that deep convection helps maintain this polynya by bringing up relatively warm CDW. This polynya tends to close again once the heat reservoir at depth is depleted (Martin et al. 2013; Behrens et al. 2016). The occurrence of open-ocean deep convection in climate models varies over decadal to multi-centennial time scales and is associated with the representation of sea ice formation and ocean stratification in individual models (Reintges et al. 2017; Latif et al. 2017). However, the exact mechanism that triggers the occurrence of OWPs in both models and the real ocean remains debated (e.g., Cheon and Gordon 2019; Kaufman et al. 2020).

Our results with a single ocean–sea ice model forced with FAFMIP perturbations show that wind forcing is the largest effect and dominates over heat and freshwater perturbations in the sSO, causing an increase of OWP events and AABW formation. This dominant response in our simulations indicates that other overly convective models might respond similarly, whereas models that usually do not form OWP might respond differently, resulting in a large spread in the AABW response. The paper is organized as follows. A description of the ocean–sea ice model, surface forcing, experimental design, and tracer budget approach is given in section 2. Changes in ocean heat content, watermass properties, MOC, and sea ice are presented in section 3. A process-based analysis of changes and their proposed mechanisms is presented in section 4. Results are discussed in the context of previous work in section 5, followed by conclusions in section 6.

## 2. Methods

We use the Australian Community Climate and Earth System Simulator Ocean Model (ACCESS-OM2; Kiss et al. 2020) with nominal horizontal resolution of  $1^\circ$  (with a Mercator refinement of  $0.25^\circ$  over the Southern Ocean) and  $50\ z^*$  levels, which includes the MOM5 ocean model (Griffies and Greatbatch 2012) and the CICE5 sea ice model (Hunke et al. 2013), coupled under the OASIS3-MCT framework (Valcke et al. 2015). We use the same spinup as Dias et al. (2020a), which brought ACCESS-OM2 to a quasi-steady state after a 1000-yr run under the climatological atmospheric state from JRA55-do v1.3 (Tsujino et al. 2018) using a repeated year (May 1984–April 1985) forcing (RYF). This particular year was chosen as it produces smaller surface salinity biases and stronger AMOC transport than other years tested (not shown), and the transition in April–May is smoother than December–January as climatological monthly

mean and variance of the climate indices are smaller in both hemispheres (K. Stewart 2018, personal communication). Control and perturbed experiments branch from a 1001 spinup and run for 80 years, as in Dias et al. (2020b). The control run was forced by the JRA55-do repeat year forcing (Stewart et al. 2020). The perturbed experiments followed the FAFMIP-protocol (Gregory et al. 2016), where surface anomalies of momentum, heat, and freshwater fluxes representative of a 2xCO<sub>2</sub> scenario from CMIP5 models (available at [fafmip.org](http://fafmip.org)) were applied to the ocean surface, in addition to the JRA55-do forcing in our ocean general circulation model (OGCM) setup. Following Dias et al. (2020b), the treatment of the salinity restoring in the control and FAFMIP experiments differs from the spinup, as explained below, while all other model configurations are exactly the same as in Dias et al. (2020a).

FAFMIP includes individual forcing experiments (namely faf-heat, faf-stress, and faf-water) and the combination of the individual changes (faf-all). The annual averaged surface momentum (STRESSp), heat (SHFp), and freshwater (SFWFp) flux perturbations south of 30°S are shown in Fig. 1. An intensification and poleward shift of the westerly winds dominate the STRESSp. The SHFp values are positive in the Southern Ocean, especially south of the New Zealand, east of the Drake Passage, and along the subpolar and subantarctic fronts in the Indian sector. Over the global ocean, the SFWFp is basically an intensification of the water cycle (Gregory et al. 2016), which includes an enhancement of the equatorial precipitation, the subtropical evaporation, and midlatitude precipitation in the ACC region. Despite the positive freshwater flux (FWF) in the sSO, the CMIP5 models used to obtain the FAFMIP flux perturbations do not include the contribution from ice sheets and likely underestimate the individual contribution from FWF.

#### a. Experimental design for FAFMIP-OGCM experiments

Even though the remaining drift in temperature and salinity is relatively small after 1000 years of spinup (Fig. 1 in Dias et al. 2020a), the control run was used to remove any remaining drift (Sen Gupta et al. 2013; Hobbs et al. 2016); therefore the results of the perturbed experiments are plotted as anomalies from the control run averaged over a specific time interval. The FAFMIP flux perturbations ( $F$ ) are monthly means (with seasonal cycle) and were held constant for 80 years using a flux adjustment method only at the ocean surface, with no direct effect on the sea ice model. The same treatment of the salinity restoring was applied to the control run and the FAFMIP experiments (faf-heat, faf-stress, faf-water, and faf-all) and is explained in detail below.

##### 1) FAF-WATER

Most OGCMs apply an SSS restoring toward climatology, which is required to avoid unrealistic model salinity drifts (Danabasoglu et al. 2014). As restoring is a nonphysical aspect of OGCMs, it is nontrivial to apply a freshwater perturbation in these models. The SSS restoring will tend to dampen the FWF perturbation, because the ocean state is modified in response to the perturbation and the difference between simulated and climatological SSS, used to the calculate restoring, also changes. Moorman et al. (2020) showed

that the reduction of the FWF perturbation due to the SSS restoring can be up to 50% in a high-resolution version of ACCESS-OM2.

Therefore, we have changed the way the SSS restoring is done in our FAFMIP experiments with an OGCM. First, we extended the spinup run for more 80 years starting from year 1001 (i.e., for the same period of the control and perturbed experiments), with no changes in the spinup setup, and saved the SSS restoring fluxes every 6 h. Second, the control and perturbed experiments were run with the SSS restoring deactivated, but applying the saved SSS restoring fluxes. This avoids damping the SFWFp in the faf-water and faf-all experiments, but preserves the effect of the SSS restoring in maintaining the model stability. By the end of the control simulation, the globally and depth-integrated temperature and salinity only increased by 0.01°C and decreased by 0.02 psu, respectively, while the AMOC showed a decrease of 2 Sv (from 14 to 12 Sv, which is within the magnitude of the AMOC natural variability in ACCESS-OM2, not shown; 1 Sv  $\equiv 10^6 \text{ m}^3 \text{ s}^{-1}$ ) at 26.5°N. Metrics in the Southern Ocean such as the MOC abyssal cell, OHC, and sea ice volume budget in the Weddell and Ross Seas were also stable throughout the control run (see section 3 and Fig. 5). Importantly, turbulent fluxes are still estimated through bulk formulas, so our approach is fundamentally different from those used in Zika et al. (2018) and Todd et al. (2020), where all boundary fluxes—including the sea ice–ocean—are prescribed. The method used in those studies assumes the sea ice state to be the same as under control (or preindustrial) conditions, while our approach allows the sea ice to evolve. As presented in section 3, changes in sea ice are an important part of the sSO response to surface perturbations.

##### 2) FAF-STRESS

For the momentum flux perturbation, both the zonal and meridional wind stress components were applied to the ocean surface. Following the FAFMIP-protocol, the STRESSp were only applied to the ocean surface (not in the sea ice) and changes in the momentum surface fluxes did not interfere in the turbulent mixing scheme. The MOM5 code was modified to incorporate these features,<sup>1</sup> where the added wind stress only perturbs the surface friction velocity but, as in our setup, it is not passed to the mixing scheme.

##### 3) FAF-HEAT

The SHFp was applied using a method allowing feedback from ocean circulation changes (Bouttes and Gregory 2014; Gregory et al. 2016) following Dias et al. (2020b). This method required modifications in the MOM5 code to include two new tracers, the added ( $T_A$ ) and redistributed ( $T_R$ ) temperatures.<sup>2</sup> The added temperature is a passive tracer which is only affected by the FAFMIP SHFp, and the redistributed temperature is only affected by the climatological forcing from JRA55-do. The redistributed temperature provides the sea surface temperature

<sup>1</sup> <https://github.com/mom-ocean/MOM5/pull/290>.

<sup>2</sup> <https://github.com/mom-ocean/MOM5/issues/199>.

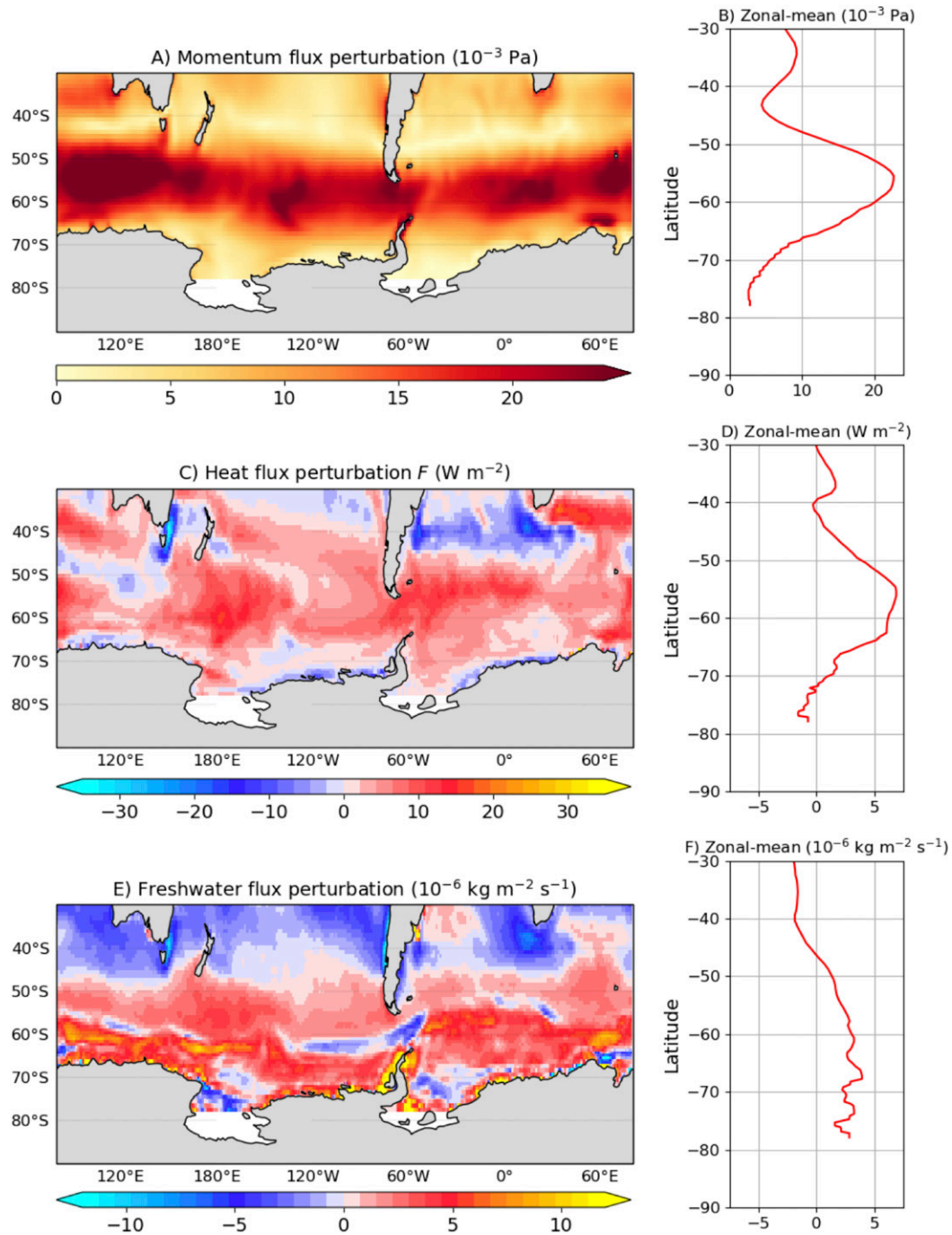


FIG. 1. (left) Maps and (right) zonal mean profiles of the annual averaged FAFMIP perturbations of (a),(b) momentum ( $10^{-3}$  Pa), (c),(d) heat ( $W m^{-2}$ ), and (e),(f) freshwater fluxes ( $10^{-6} kg m^{-2} s^{-1}$ ).

(SST) field for the bulk formula calculations in *faf-heat* and *faf-all* experiments instead of the OGCM prognostic surface Conservative Temperature ( $\Theta$ ), to avoid the negative feedback that occurs when the FAFMIP heat flux perturbation is applied to the SST (Gregory et al. 2016). As earlier adopted for other FAFMIP simulations [using the GFDL-ESM2M atmosphere–ocean general circulation model (AOGCM), which is also

MOM5-based], our implementation accounts separately for the frazil ice formation due to  $\Theta$  and  $T_R$ , meaning that the net heat flux applied to these tracers is not exactly equal, although differences are small. This approach, however, prevents the prognostic temperature ( $\Theta$ ) from falling below the freezing point, so that no modification to the equation of state is necessary (Gregory et al. 2016).



### b. Ocean heat budget

The contribution to the heat content time tendency in a grid cell, per unit horizontal area, from individual physical processes is represented by Eq. (1), as in [Dias et al. \(2020a\)](#):

$$c_p \rho_0 \frac{\partial(\Theta dz)}{\partial t} = -c_p \rho_0 (\nabla_H \cdot \mathbf{F} + \partial_z \mathbf{F}^z) dz. \quad (1)$$

This approach allows the contribution from individual processes [ $\mathbf{F}$ , RHS of Eq. (1)] to the time change in ocean heat content [LHS of Eq. (1)] to be determined. Here,  $\rho_0$  is the reference density ( $1035 \text{ kg m}^{-3}$ ) and  $c_p$  is the heat capacity of seawater ( $3992 \text{ J kg}^{-1} \text{ }^\circ\text{C}^{-1}$ ). The term  $\mathbf{F}$  includes the resolved advection ( $u\Theta$ ) and also subgrid-scale processes, where  $\nabla_H$  is the horizontal divergence operator and  $\partial_z$  is the vertical partial derivative of the vertical components of individual heat transport processes  $\mathbf{F}^z$ . The individual contributions to the heat budget ( $\mathbf{F}$  and  $\mathbf{F}^z$ ) include the surface fluxes (SFC) and oceanic processes such as advection (ADV), dianeutral (across neutral surfaces) diffusion (DIA), the nonlocal  $K$ -profile parameterization term [KPP; following [Large et al. \(1994\)](#)], penetration of shortwave radiation (SWP), mesoscale eddy-related transports (EIT), restratification of the mixed layer due to submesoscale eddies (SUB), convection (CON), heat exchange related to watermass transfer from precipitation-minus-evaporation (PME), river runoff (RIV), and heat flux due to frazil ice formation (FRZ):

$$\mathbf{F} = \text{SFC} + \text{ADV} + \text{DIA} + \text{KPP} + \text{SWP} + \text{EIT} + \text{SUB} \\ + \text{CON} + \text{PME} + \text{RIV} + \text{FRZ}. \quad (2)$$

A detailed description of the processes in  $\mathbf{F}$  and their role in the mean state are presented in [Dias et al. \(2020a\)](#). In steady state, the global ocean heat transports exhibit a balance between distinct processes ( $\mathbf{F}$ ) presented in Eq. (2). While previous studies showed that the large-scale advection (ADV) and mesoscale eddy-induced transport (EIT) are the main contributors to this global balance ([Gregory 2000](#); [Banks and Gregory 2006](#); [Kuhlbrodt et al. 2015](#); [Griffies et al. 2015](#)), a different perspective based on the superresidual transport was introduced by [Kuhlbrodt et al. \(2015\)](#) and further explored ([Dias et al. 2020a](#); [Saenko et al. 2021](#); [Savita et al. 2021](#)). The superresidual transport (SRT) is given by the superposition of the large-scale advection and eddy-induced transport ( $\text{SRT} = \text{ADV} + \text{EIT}$ ), and it has opposing effects in deep mixed layers (the mid- to high-latitude winter mixed layer, usually a couple hundred meters deep) and in the ocean interior (regions below the winter mixed layer depth).

The two depth-dependent regimes of the SRT are summarized as follows [for a schematic see Fig. 13 in [Dias et al. \(2020a\)](#)]. In deep mixed layers, the SRT compensates upward heat fluxes by processes that create dense watermasses, such as convection and vertical mixing, by transporting heat downward. In the ocean interior, the SRT acts to move these waters into their respective neutral layers, generally reflected in upward heat and salt fluxes balanced by dianeutral mixing. Therefore, the ocean interior regime can be interpreted as the classical diffusive–advective balance ([Stommel and Arons 1960](#); [Munk 1966](#)), where the SRT represents the advection component, with the important difference

that the diffusion is enhanced at rough topography as proposed by recent theories ([Ferrari et al. 2016](#); [McDougall and Ferrari 2016](#); [Holmes et al. 2018](#)). Given that the SRT framework elucidates the regions of watermass formation in the heat budget analysis, we will take advantage of this framework to evaluate the drivers of changes in AABW formation and transport in [section 4](#).

### 3. Ocean heat content changes

First the response of the sSO to the FAFMIP perturbations is evaluated in terms of depth-integrated ocean heat content (OHC) and zonal-mean temperature anomalies ([Fig. 2](#)). Each forcing perturbation makes a significant contribution. Intensification and poleward migration of the westerlies (faf-stress; [Fig. 2a](#)) causes a decrease in OHC, while OHC increases due to positive SHFp (faf-heat; [Fig. 2c](#)) and positive SFWFp (faf-water; [Fig. 2e](#)). These responses are similar to those obtained by the ensemble-mean AOGCMs-FAFMIP in [Gregory et al. \(2016\)](#) (their Figs. 7 and 9). The largest cooling in faf-stress is located in the Weddell Sea, followed by the cooling in the Ross and Amundsen Seas. It is worth noting that the spatial distribution of the (extra) cooling shows cold water extending equatorward, indicating paths of export of cold water in the Atlantic and Pacific sectors. Increases in OHC in faf-heat and faf-water are larger in the Weddell Sea than elsewhere in the sSO. South of  $60^\circ\text{S}$ , the zonal mean temperature anomalies ([Fig. 2](#), right column) show that the cooling in the faf-stress is larger than the warming in faf-heat and faf-water, and it is transported northward above the ocean bottom. The response in the faf-all experiment approximates the sum of individual responses (with a small contribution from nonlinear interactions); [Fig. 2g](#) shows that the cooling from faf-stress dominates over the warming from faf-heat and faf-water. OHC increases over the Antarctic shelf in faf-all, suggesting that heat and freshwater forcing dominates ([Figs. 2d,f,h](#)); however, the spatial pattern depends on the time interval chosen, as the processes that cause cooling have significant interannual and decadal variability over the course of the experiment as explained below. The cooling signal deeper than 2000 m in [Fig. 2h](#) is the result of advection of bottom waters formed in previous years (e.g., the Weddell Polynya occurs in faf-all from years 50 to 65; see [Fig. 5](#)).

The OHC changes described above reflect the mechanisms of AABW formation in ACCESS-OM2. As found in several other coarse model simulations, large OWP occur in the Southern Ocean in the control run, especially associated with the Weddell and Ross Gyres ([Dias et al. 2020a](#)). Within the modeled OWP, low sea ice concentration allows exchange of heat between the relatively warm and salty deep waters (upwelled in the Antarctic Divergence) with the cold overlying atmosphere. This exchange drives heat out of the ocean, which triggers the deep convection (more details in [section 4](#)), resulting in very deep mixed layers ([Fig. 3a](#)). Deep open-ocean convection in the Weddell Sea is rarely observed ([Zwally and Gloersen 1977](#); [Gordon and Comiso 1988](#); [Campbell et al. 2019](#)) but is common in many large-scale ocean climate models, where the deep open-ocean convection is the main mechanism of AABW formation ([Heuzé et al. 2015](#)). In response to changes in winds, the sea ice cover decreases at most regions, allowing venting of ocean heat at deep mixed layers ([Figs. 3c,d](#)).

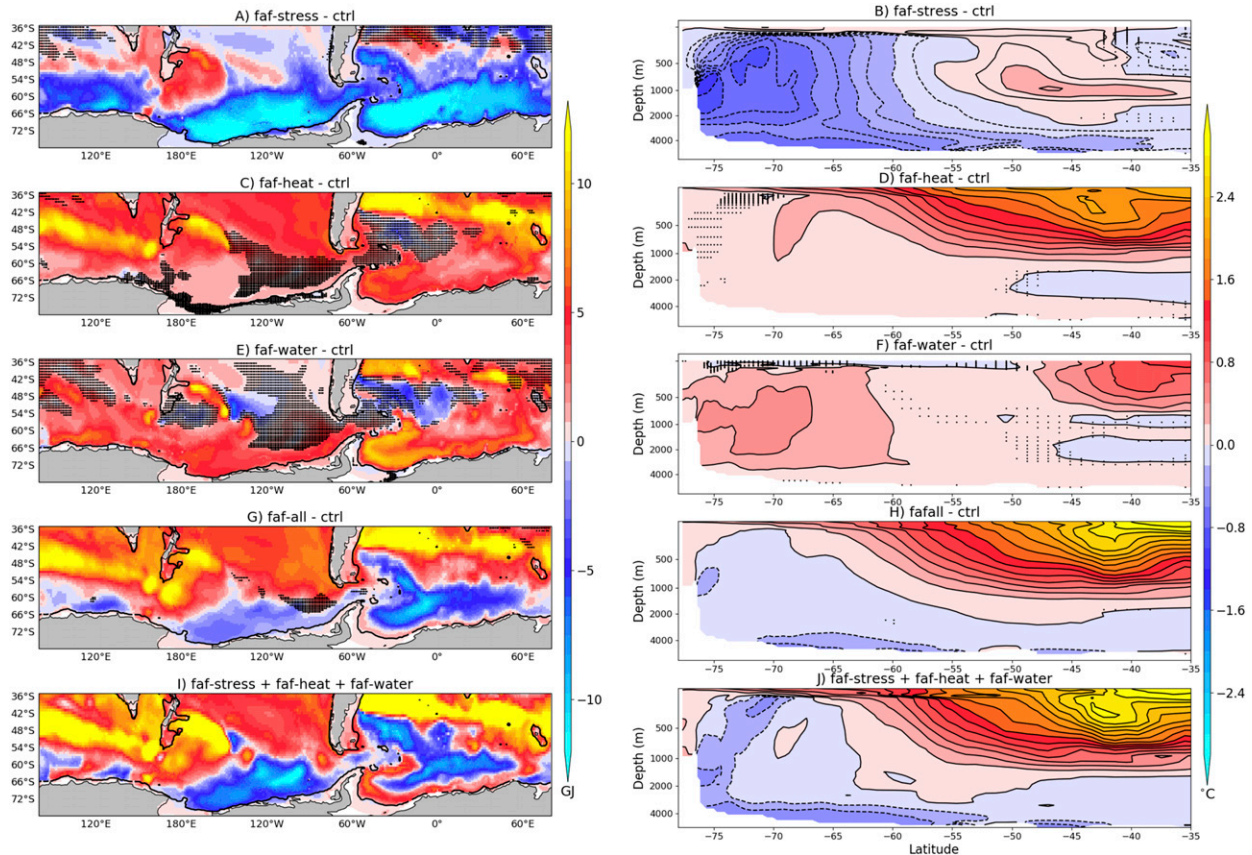


FIG. 2. Time mean of years 1061–80 of the FAFMIP experiments relative to the control: (left) change in ocean heat content ( $\text{GJ m}^{-2}$ ; the vertical integral of the change in the ocean temperature multiplied by the volumetric heat capacity) and (right) change in zonal-mean temperature: (a),(b) faf-stress, (c),(d) faf-heat, (e),(f) faf-water, and (g),(h) faf-all. (i),(j) The sum of individual experiments (faf-stress, faf-heat, and faf-water) to highlight the nonlinear response in comparison to faf-all. Black contours in the left panels represents the 1000-m isobath. Regions where the standard deviation of the FAFMIP simulations are smaller than 1.96 times the standard deviation of the control run are represented by a black stippling (i.e., 95% confidence interval).

In contrast, the SHFp and SFWFp drive an increase of sea ice and shallowing of the mixed layers (Figs. 3e,f,g,h). The faf-all experiment shows significant sea ice reduction and expansion of the Ross and Weddell Polynyas (Figs. 3i,j), indicating that the wind changes dominate the all forcing response.

Although climate/ocean models have a limited representation of the complex mechanisms of AABW formation over the shelf, they can still have a good representation of the bottom water properties (Heuzé et al. 2013). As with every model, biases are expected and reflect on the watermass structures. The Conservative Temperature–salinity ( $\Theta$ – $S$ ) diagrams (black “x” in Figs. 4a,c,e,g) for ACCESS-OM2 reproduces the main features seen in the *World Ocean Atlas 2018* (WOA18) climatology (Locarnini et al. 2018; Zweng et al. 2018) (Figs. 4b,d,f,h). The main difference is in the open ocean, where both Weddell and Ross regions have less Weddell Sea Deep Water (WSDW) and Circumpolar Deep Water (CDW) in ACCESS-OM2 than seen in observations (Figs. 4c,d,g,h), resulting in a persistent cold bias. Some differences are also noticed within near-freezing temperatures, where Winter Waters (WW) from ACCESS-OM2 are generally colder (warmer) in the Ross (Weddell) Sea

than in WOA18. The Weddell Sea Bottom Water (WSBW) and the Ross Sea Bottom Water (RSBW) are regional varieties of AABW, with temperatures below  $-0.5^{\circ}\text{C}$  and salinity larger than 34.5, localized at depths greater than 3000 m. The WSBW and RSBW result from the mixing between shelf waters (with near-freezing temperatures) and warm deep waters (WSDW and CDW,  $\Theta > -0.5^{\circ}\text{C}$  and  $S > 34.5$ ; Kerr et al. 2018). Shelf waters are not expected to be well represented given the model resolution (varying from  $1^{\circ}$  to  $0.25^{\circ}$  over the Southern Ocean); nevertheless, our results indicate that both low-salinity ( $S < 34.4$ , the model representation of WW) and high-salinity waters ( $S > 34.65$ , equivalent to HSSW) are found over the continental shelf (Figs. 4a,e).

Watermass precursors of AABW (HSSW) and regional varieties of bottom water (WSBW and RSBW) are sensitive to the FAFMIP perturbations. In faf-stress, HSSW salinity increases in the Weddell and Ross Seas, resulting in denser WSBW, RSBW, and AABW (green dots at the left column of Fig. 4). The opposite response occurs in faf-water (blue dots in Fig. 4), where HSSW salinity decreases, resulting in lighter waters at depth, in both the Weddell and Ross Seas. The faf-heat response is an overall

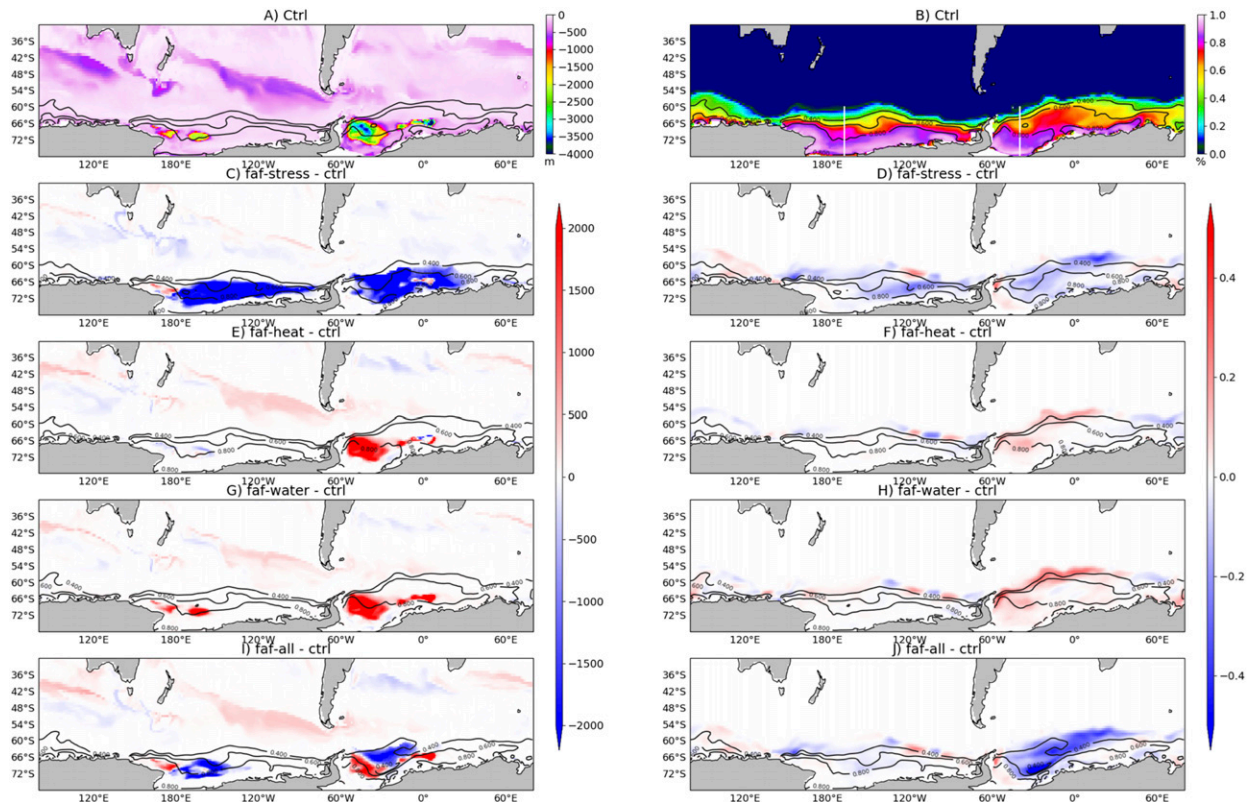


FIG. 3. September mean (left) ocean mixed layer depth (m) for years 1061–80, using a reference density anomaly of  $0.003 \text{ kg m}^{-3}$  relative to the surface following Downes et al. (2015), and (right) sea ice concentration with contours of 40%, 60%, and 80% for (a), (b) the control, and also the FAFMIP experiments (c), (d) faf-stress, (e), (f) faf-heat, (g), (h) faf-water, and (i), (j) faf-all. Positive (negative) MLD and sea ice concentration anomalies are denoted by red (blue) colors in (c)–(j). White lines in (b) define the sections at the Ross and Weddell Seas used in the analyses presented in Figs. 4, 5b–g, and 6.

warming (Fig. 4, red dots); however, the HSSW and RBSW properties in the Ross Sea are fairly similar to the control run (and thus red dots are behind black “x”), as changes in the Ross Sea in faf-heat are minor (cf. Figs. 3a,e). In the Weddell Sea, the faf-heat  $\Theta$ – $S$  properties are clearly warmer than in the control run, although changes in density are not substantial due to the dominant salinity effect at these temperatures. The faf-all experiment shows a mixed response in  $\Theta$ – $S$  space (Fig. 4), generally dominated by increased density due to faf-stress partially compensated by the opposite contributions from faf-heat and faf-water. These  $\Theta$ – $S$  property changes agree well with the anomalous surface heat and freshwater fluxes (see section 4a); salinification (freshening) at the continental shelf are linked with negative (positive) surface freshwater fluxes, while cooling (warming) in the open ocean is caused by increased (decrease) of the surface heat loss (Fig. 8).

Temporal variability of the sSO response is investigated through the evolution of the MOC, the depth-integrated OHC and sea ice changes (Fig. 5). The abyssal MOC (south of  $60^{\circ}\text{S}$  and below 500 m) has large positive anomalies in the faf-stress and faf-all experiments, albeit highly time-dependent due to expansion and contraction of the OWP, and small but constant negative anomalies in faf-water (Fig. 5a). The temporal variations in the MOC are primarily explained by the changes in the OHC depth-integrated below 500 m and meridionally averaged along the Weddell and

Ross Seas sections (Figs. 5b,c). Deep open-ocean convection causes cooling of the entire column (Figs. 6b,e,g,j), which breaks the stratification and ventilates the middepth heat reservoir. When the deep open-ocean convection event ceases (e.g., after year 1015 in Fig. 6b), heat starts to build up again at middepths, likely associated with southward transport of CDW. In contrast, in experiments where the OHC increases during the simulation (faf-heat and faf-water, Figs. 5b,c), the vertical stratification gradually intensifies throughout the simulation (Figs. 6c,d,h,i).

Insights on the mechanisms that trigger the OWP response to wind changes are obtained through the sea ice volume budget, where the volume tendency is decomposed into the contributions from thermodynamics and dynamics (including lateral advective and ridging redistribution); positive (negative) values denote local ice growth (melting). The sea ice budget is presented for the faf-stress and faf-all experiments in Figs. 5d,e,f,g, averaged for the month of June (representing sea ice growth in winter) and meridionally for the same sections in Fig. 3b. There is a clear link between sea ice tendency and the variability of the MOC and the OHC (Fig. 5). While high rates of sea ice growth are expected during winter, it is substantially smaller during the OWP events (e.g., years 1005–08 in the Weddell Sea and 1010–30 in the Ross Sea, in faf-stress). The thermodynamical effect dominates during the early years of OWP events, indicating inhibition of sea ice



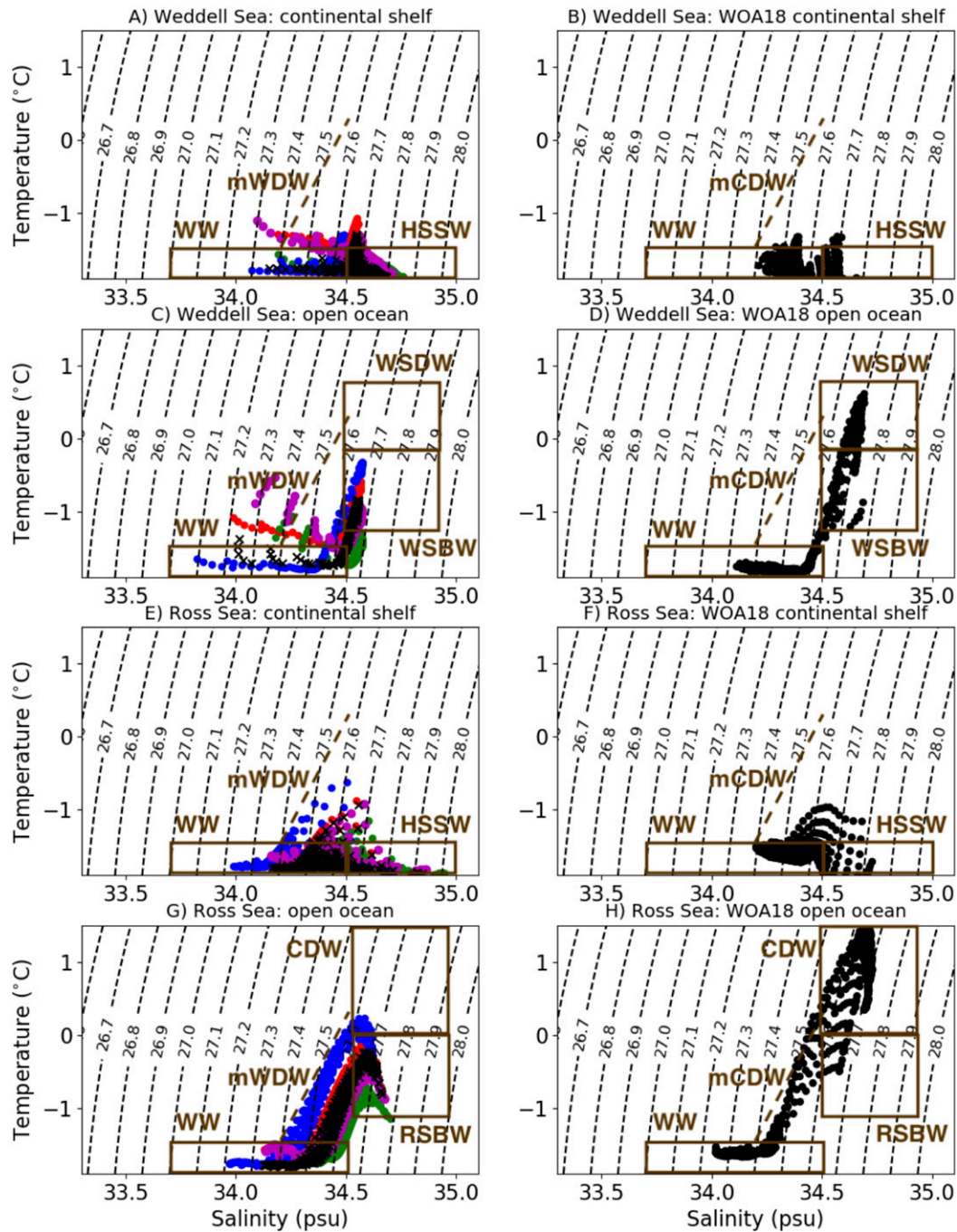


FIG. 4.  $\Theta$ - $S$  diagrams averaged for years 1061–80 in the (a)–(d) Weddell Sea (transect at  $40^{\circ}\text{W}$ ) and (e)–(h) Ross Sea (transect at  $175^{\circ}\text{W}$ ) regions, for continental shelf (depths shallower than 1000 m) in (a), (b), (e), and (f) and open-ocean grid points (depths deeper than 1000 m) in (c), (d), (g), and (h). (left) ACCESS-OM2, where the control run is represented by black x marks, faf-stress by green circles, faf-heat by red circles, faf-water by blue circles, and faf-all by magenta circles. (right) Climatological  $\Theta$ - $S$  diagrams from the *World Ocean Atlas 2018* (Locarnini et al. 2018; Zweng et al. 2018) at  $40^{\circ}\text{W}$  [in (b) for continental shelf and (d) for open ocean] and at  $175^{\circ}\text{W}$  [in (f) for continental shelf and (h) for open ocean] for comparison. Boxes represent estimates of the watermass intervals based on observations (Kerr et al. 2012, 2018): Winter Water (WW), High Salinity Shelf Water (HSSW), Weddell Sea Deep Water (WSDW), Weddell Sea Bottom Water (WSBW), modified Warm Deep Water (mW/DW), Circumpolar Deep Water (CDW), Ross Sea Bottom Water (RSBW), and modified Circumpolar Deep Water (mCDW).



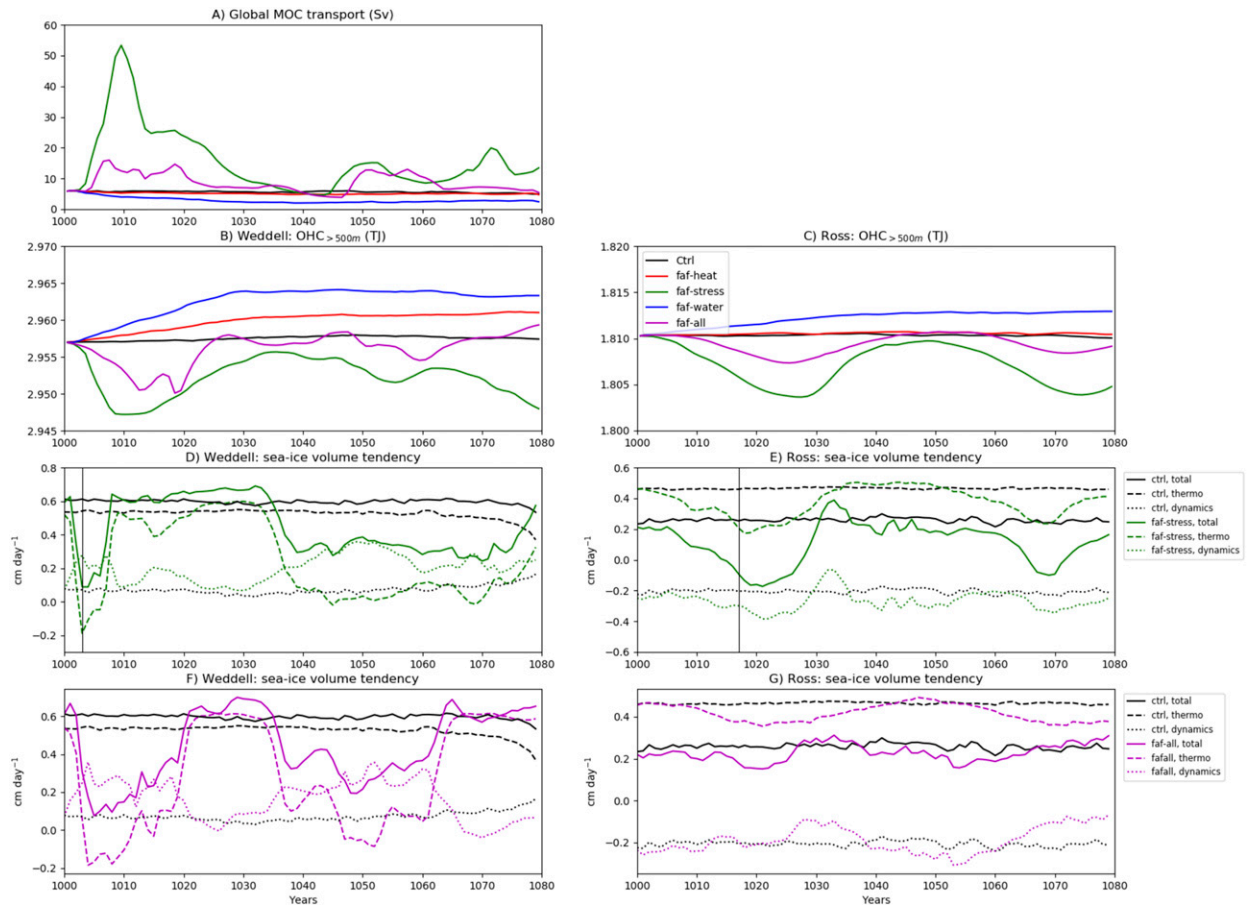


FIG. 5. (a) Time series of the maximum transport (Sv) of the global MOC abyssal cell south of  $60^{\circ}\text{S}$ , below 500 m. (b),(c) The meridionally averaged, depth-integrated (500 m to bottom), OHC (TJ) for the Weddell and Ross Sea sections as shown in Fig. 3b. (d)–(g) The sea ice volume budget (total tendency: solid line, thermodynamic component: dashed line, dynamic/transport component: dotted line;  $\text{cm day}^{-1}$ ) for the same sections, meridionally averaged at grid points where depth is greater than 1000 m. Control experiment shown in black and FAFMIP experiments are shown as: faf-heat (red), faf-stress (green), faf-water (blue), and faf-all (magenta). The vertical black lines in (d) and (e) show the years chosen to show the maps of the sea ice budget in Fig. 7.

growth by anomalously warm waters near-surface, with some compensation arising from dynamical effects in the Weddell Sea. The interaction of these waters with the cold atmosphere results in heat loss and deep open-ocean convection. The spatial distribution of the sea ice budget components (Fig. 7), is shown as June average of years 1003 (for the Weddell OWP) and 1017 (for the Ross OWP, vertical black lines in Figs. 5d,e), representing the first OWP events in the Weddell and Ross Seas, respectively. Around the regions where the OWP are expanding, the thermodynamical contribution is near zero or negative (see black contours in Figs. 7e,f), while other areas mostly see sea ice growth (due to positive thermodynamical effect). As STRESSp does not affect the mixing scheme (section 2), these results suggest that upwelling of warm deep waters is likely the trigger and primary driver of these OWP events.

#### 4. Drivers of OHC changes

In this section we evaluate the drivers of OHC changes through a heat budget analysis. The ventilation of the deep SSO

occurs through the transformation of upwelled CDW into dense waters by addition of salt and/or loss of heat—that is, formation of AABW (e.g., Carmack and Foster 1975). The superresidual transport (SRT) framework describes the connection between physical processes associated with the formation and recirculation of dense waters within an ocean climate model (Dias et al. 2020a), and therefore is adopted here to investigate the changes in AABW formation in our perturbation experiments.

##### a. Surface heat and freshwater fluxes

Air–sea exchange is diagnosed using net surface heat and freshwater fluxes. At high latitudes, the presence of sea ice inhibits interaction between the ocean surface and the atmosphere. In the control state, surface heat loss occurs over most of the SSO region. The surface freshwater flux (FWF), which also includes salt fluxes converted to equivalent freshwater fluxes, is dominated by the sea ice component in ACCESS-OM2, with secondary contribution from net precipitation (Dias et al. 2020a); this model, however, does not include ice sheets, calving,

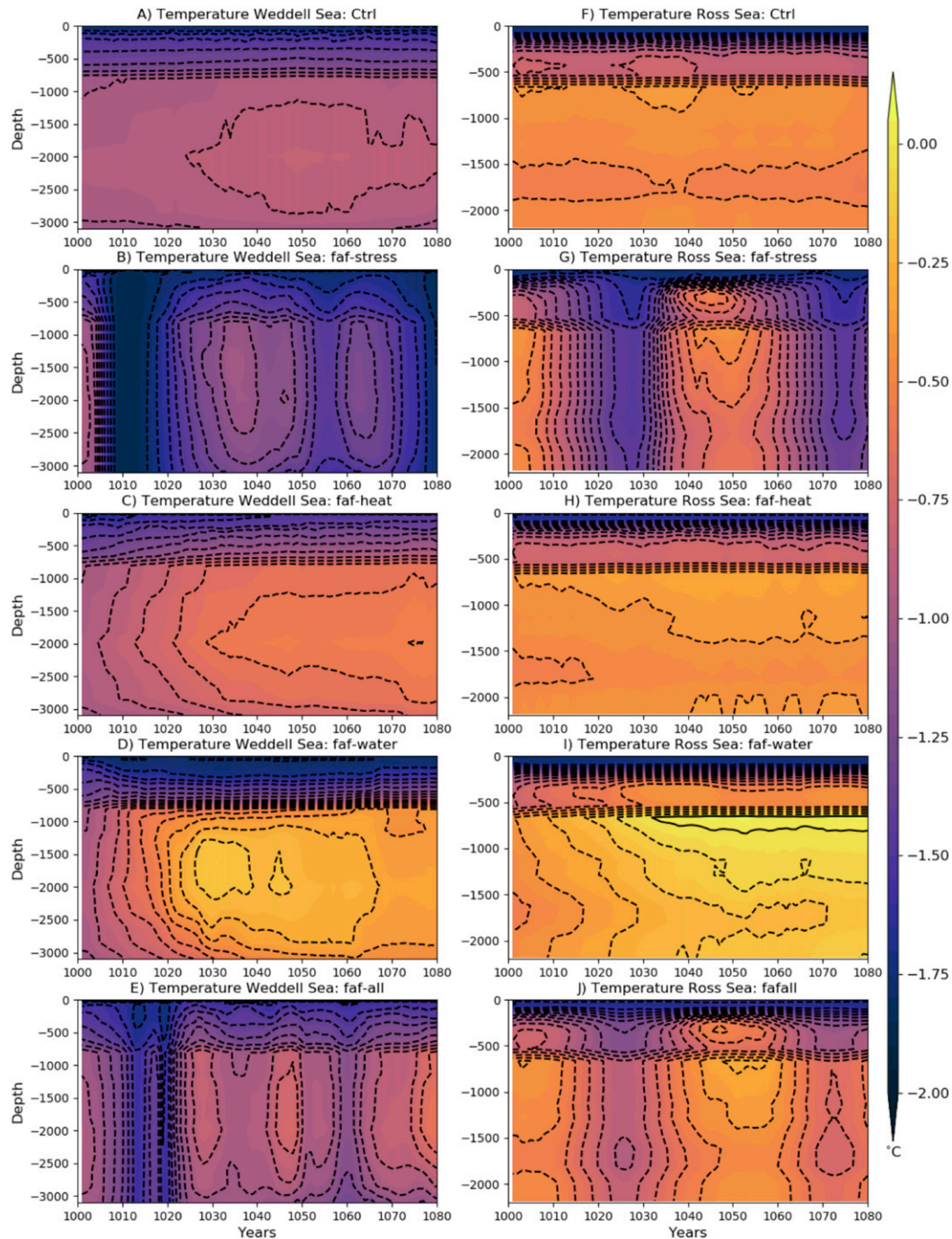


FIG. 6. Meridionally averaged temperature ( $^{\circ}\text{C}$ ) over the (left) Weddell and (right) Ross Seas sections as shown in Fig. 3b, for (a),(f) the control experiment, (b),(g) faf-stress, (c),(h) faf-heat, (d),(i) faf-water, and (e),(j) faf-all.

or icebergs. On the Antarctic continental shelf, negative FWF occurs due to positive salt inputs associated with brine rejection from sea ice formation. In contrast, at the marginal ice zone, sea ice melting dominates the positive FWF (Fig. 8b).

In the sSO, the decrease of sea ice coverage in faf-stress and faf-all, associated with the expansion of the OWP (Figs. 3d,i), enhances air–sea exchange. In the Weddell and Ross Gyres

surface heat loss is much larger in faf-stress and faf-all than in the control run (Figs. 8a,c,i), reflecting venting of heat from the deep ocean during OWP events (Figs. 6b,e,g,j), and leading to an abrupt increase in abyssal MOC (Fig. 5a). Different timing of OWPs in the Weddell and Ross Seas, while the STRESSp is similar across these sectors (Fig. 1a), suggests that the precondition ocean state (e.g., stratification; Figs. 6a,b) plays a role

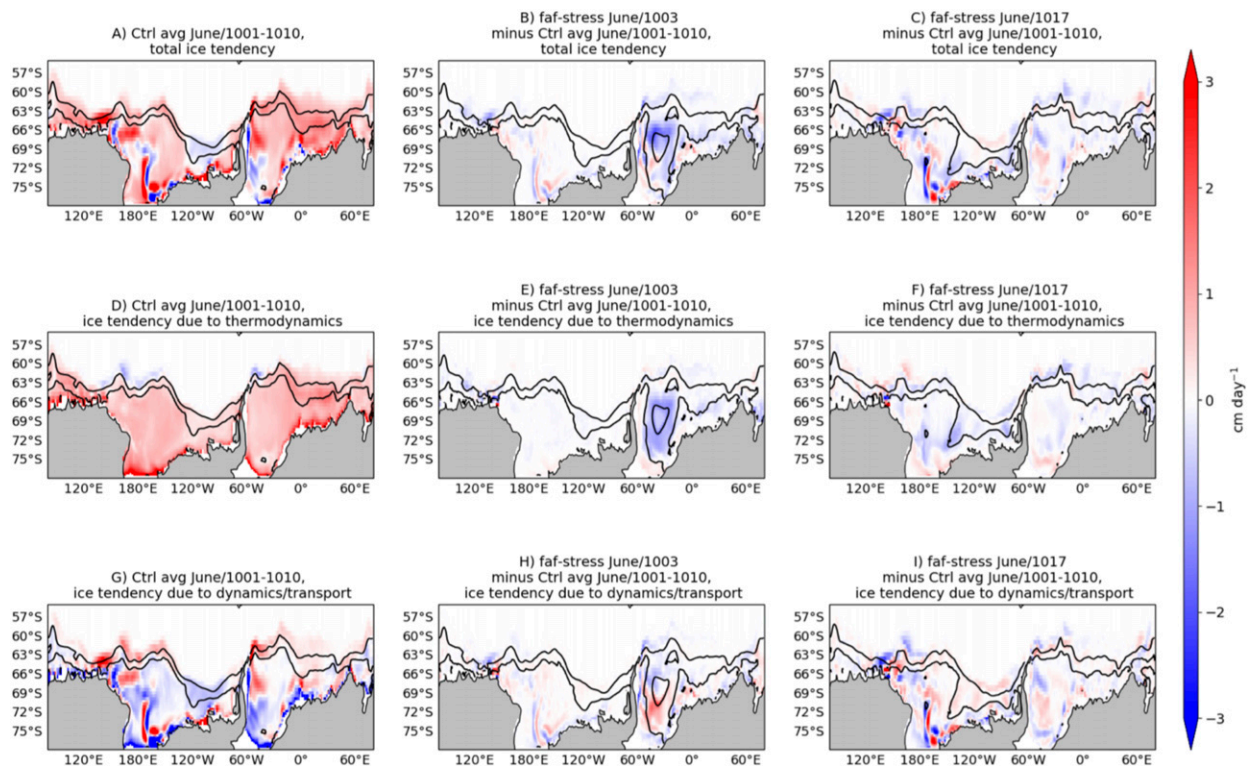


FIG. 7. Sea ice volume budget: (top) total tendency, (middle) thermodynamic contribution, and (bottom) dynamic/transport contribution ( $\text{cm day}^{-1}$ ). (left) The control experiment is presented as an average of the month of June for the first 10 simulated years (1001–10). (center) Monthly mean anomalies sea ice budget for June 2003 (relative to the control run averaged over June 1001–10), when the Weddell polynya opens for the first time in the faf-stress experiment (vertical line in Fig. 5d). (right) Monthly mean anomalies sea ice budget for June 2017 (relative to the control run averaged over June 1001–10), when the Ross Polynya opens for the first time in the faf-stress experiment (vertical line in Fig. 5e). Black contours are the sea ice concentration at 50% and 90%. In general, blue colors indicate sea ice melting (or local decrease of sea ice thickness) and red colors indicate sea ice growth (or increase of sea ice thickness).

in the development of the deep convection events. In contrast to the open ocean, a small decrease of heat loss occurs over the Weddell and Ross continental shelf (Figs. 8c,i), arising from slightly increased sea ice concentration (Figs. 3d,j). The effect of the momentum perturbation in the OHC and in the surface heat fluxes occurs via redistribution of the unperturbed temperature fields (Banks and Gregory 2006; Xie and Vallis 2012; Garuba and Klinger 2016), where the OWP allows ocean heat loss to the atmosphere and deep convection. Differences in the anomaly of surface heat flux between faf-all (Fig. 8i) and from FAFMIP (ensemble mean of 13 CMIP5 models; Fig. 1b) suggests that ocean heat loss via OWP is not necessarily a rule in AOGCMs. However, this comparison can be affected by the potentially distinct sSO response in AOGCMs (e.g., models with OWPs might respond to momentum perturbation as ACCESS-OM2, while models without OWPs might respond differently); due to distinct time-averaging (years 1001–80 in ACCESS-OM2, years 61–80 in AOGCM-1pctCO2 simulations for FAFMIP), a substantial reduction of the surface heat loss in faf-all in the Weddell Sea is observed in ACCESS-OM2 when averaging over years 1061–80 (not shown) because the OWP is absent (Fig. 5b).

The surface FWF of faf-stress shows a distinct regional distribution (Fig. 8d). Positive freshwater anomalies occur in the

center of the Weddell and Ross Gyres, where sea ice concentration decreases (Fig. 3d), likely caused by strengthening of sea ice melting in summer, and reduction of sea ice formation in winter (i.e., less brine rejection). On the Antarctic shelf, negative FWF anomalies are found in Weddell Sea (west of 20°W), where sea ice increases, and positive FWF anomalies occur in patches from 20°W to 70°E and between 100° and 150°E, where sea ice decreases (Fig. 3d). While the response in the open ocean is dominant in ACCESS-OM2, changes over the Antarctic shelf might indicate how a more realistic sSO (where AABW forms in coastal polynyas) would respond to climate change.

Positive SHFp and SFWFp applied to the sSO in faf-heat and faf-water (Figs. 1b,c) cause in general an opposite response in net surface heat and freshwater fluxes to that found in faf-stress. However, significant differences between faf-heat and faf-water are observed in the Weddell and Ross Seas. While the surface heat flux anomaly is positive in both experiments (Figs. 8e,g), the Ross Sea has positive (negative) anomalies in faf-water (faf-heat). This relates to the fact that the Ross Polynya is not affected by the SHFp: deep MLD still occurs as in the control run (but vanishes due to SFWFp, Figs. 3a,e,g) and the changes in OHC are less significant than in faf-water



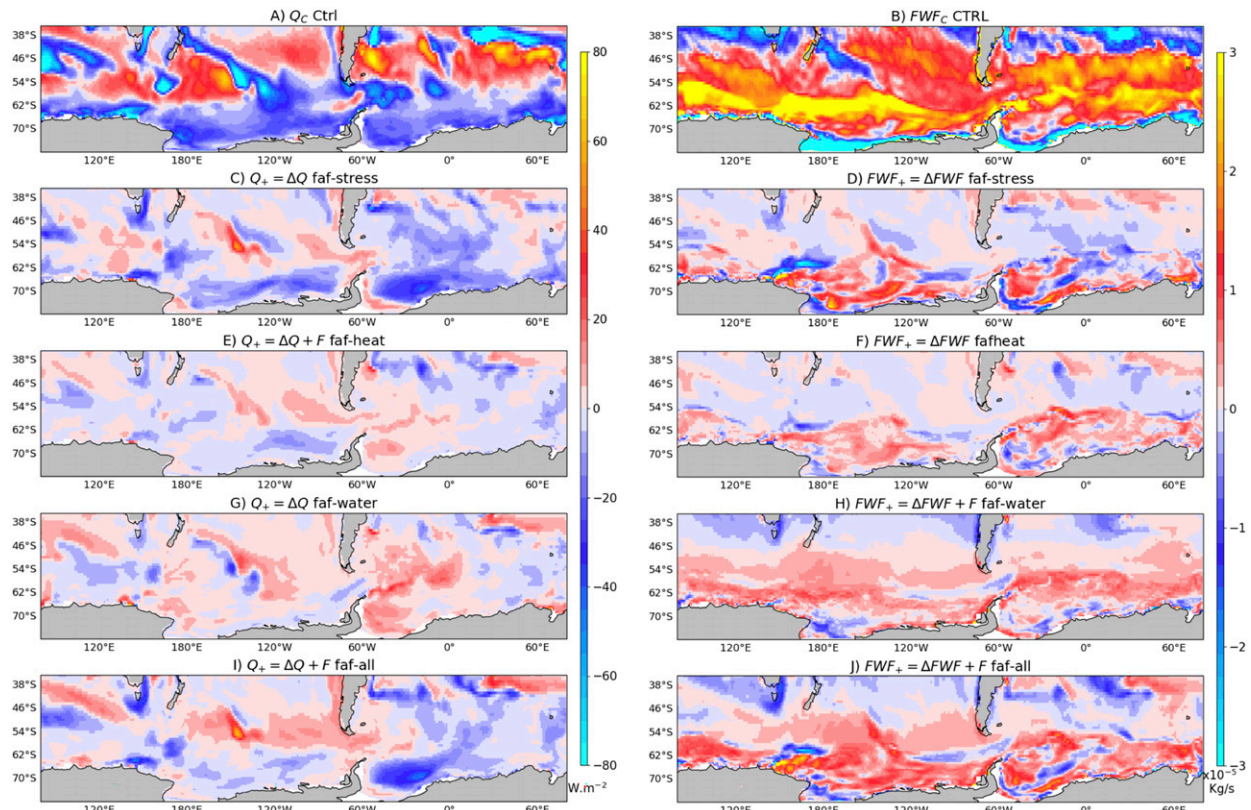


FIG. 8. Time-mean (years 1001–80) ocean surface (left) heat ( $\text{W m}^{-2}$ ) and (right) freshwater ( $10^{-5} \text{ kg s}^{-1}$ ) fluxes in (a),(b) the control experiment (absolute values), (c),(d) faf-stress, (e),(f) faf-heat, (g),(h) faf-water, and (i),(j) faf-all (anomalies with reference to the control run).

(Fig. 5c). Anomalous surface heat and freshwater fluxes in faf-all are dominated by response to STRESSp, although the faf-water and faf-heat also contribute substantially (Figs. 8i,j).

### b. Ocean heat transport

In the control run (when averaged over the entire simulation, years 1001–80), the sSO cools on average in most Southern Ocean sectors (Figs. 9a, 10a, and 11a). In the Atlantic and west Pacific sectors (eastern and western Pacific sections are separated at  $130^{\circ}\text{W}$ ), these negative heat tendencies are associated with a weak cooling drift due to the strong AABW formation in the Weddell and Ross Seas, where cooling tendencies from surface boundary layer processes dominate: convection (CON), nonlocal KPP, and submesoscale eddies (SUB), as shown in Figs. 9c and 10c (we will refer to this as convection hereafter for simplicity, as it is the dominant component). As these sectors exhibit large OWP and deep mixed layers (Figs. 3a,b), these surface boundary layer processes are stronger off the shelf ( $>1000 \text{ m}$ ), but also significant at the continental shelf (depths  $<1000 \text{ m}$ ), indicating that shelf processes might also drive bottom water formation processes. Lago and England (2019) estimated, using a previous version of ACCESS-OM, that the AABW formation is 44% due to open-ocean convection and 56% due to shelf convection. Dianeutral mixing (DIA) also generally cools these regions but is less important (not shown), and therefore is combined with the surface boundary layer processes in Figs. 9c,

10c, 11c, and 12c. The SRT has a warming effect and counterbalances the cooling due to surface boundary layer and DIA processes (Figs. 9b and 10b). While surface boundary layer processes mostly cool the sSO, the opposite is seen between 500 and 1000 m near the shelf break in the Atlantic and west Pacific sectors (Figs. 9b,c and 10b,c); dominated by KPP and CON (not shown), this relates to the vertically rearrangement of heat associated with overturning, as warm waters sitting at depth are transported upward while cold waters sink to larger depths.

The SRT effectively removes newly formed dense waters from deep mixed layers and transports them to the ocean interior (Dias et al. 2020a). The opposite heat convergence from SRT, in the deep mixed layers opposed to the ocean interior, reflects this mechanism (see Fig. 13 in Dias et al. 2020a). In the deep mixed layers, the SRT opposes the cooling from convection, while in the ocean interior the SRT has a cooling effect (as cold dense water is advected along isopycnals) and counterbalances the warming from DIA. As suggested by the classical advective–diffusive theory, the globally integrated heat budget in the ocean interior (north of  $65^{\circ}\text{S}$  and below 2000 m in Fig. 9) is dominated by upward heat convergences (i.e., cooling) from SRT (considered as the “advective” component, Fig. 9b) balanced by downward heat convergences (warming) from DIA (Fig. 9c). While the balance between SRT and convective processes in deep mixed layers represents watermass formation, the balance between

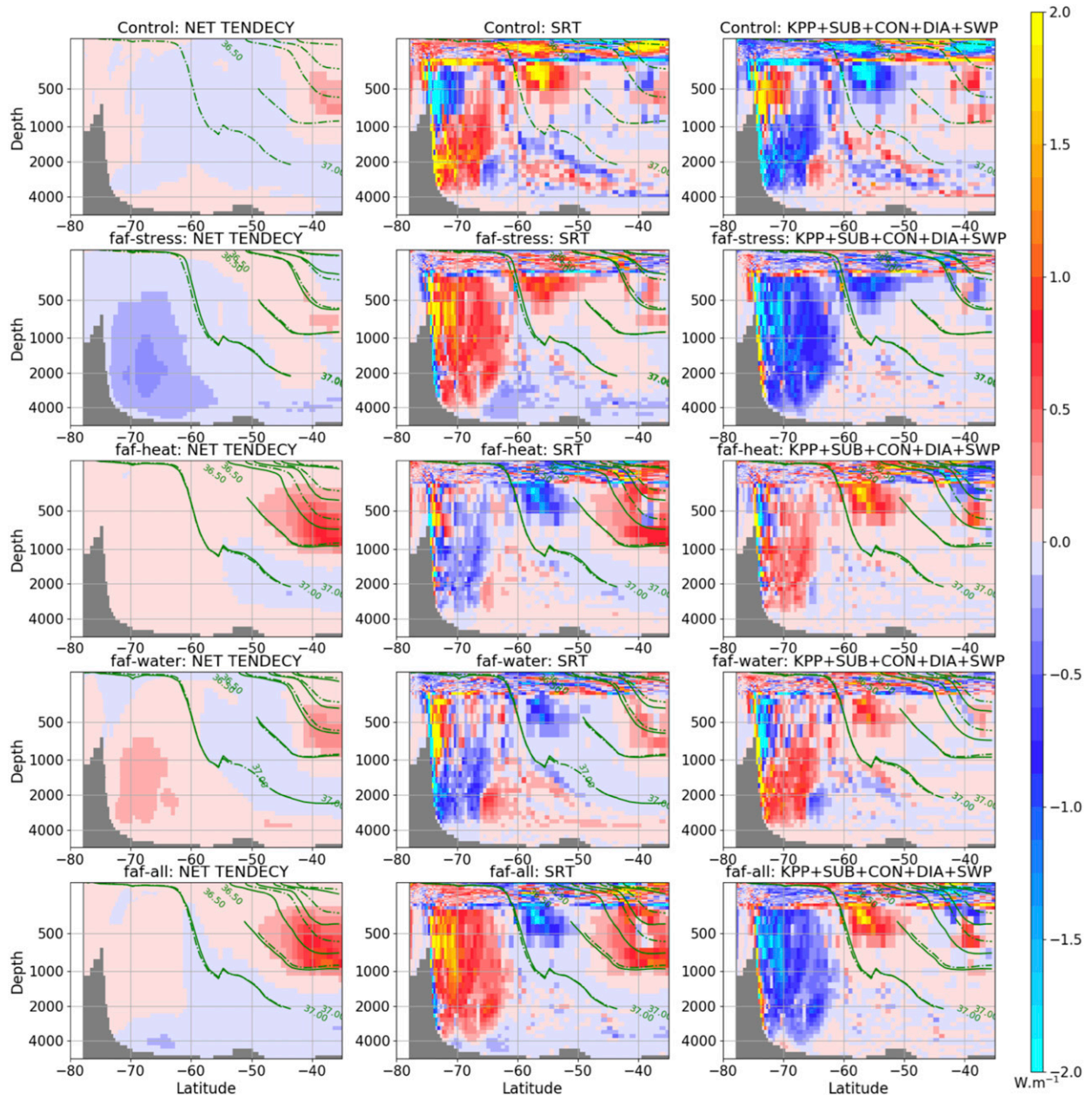


FIG. 9. Time-mean (years 1001–80), zonally integrated ocean heat flux convergences ( $\text{W m}^{-1}$ ) for the control and FAFMIP experiments in the Atlantic sector ( $70^{\circ}$ – $20^{\circ}$ W) of the Southern Ocean, for (a)–(c) the control run, and for the FAFMIP experiments (anomalies relative to the control run): (d)–(f) faf-stress, (g)–(i) faf-heat, (j)–(l) faf-water, and (m)–(o) faf-all. (left) The net heat tendency (NET), (center) the heat convergence due to the superresidual transport (SRT), and (right) the heat convergence due to the combination of mixed-layer (KPP, SUB, CON), diapycnal diffusion (DIA), and shortwave penetration (SWP) processes. As expected from a closed budget,  $\text{NET} = \text{SRT} + (\text{KPP} + \text{SUB} + \text{DIA} + \text{SWP})$ . Green isopycnals show  $\sigma_2$  density contours following Downes et al. (2015).

SRT and DIA relates to the recirculation and erosion of bottom waters, by slowly mixing with the relatively warmer deep waters sitting above. The export of AABW (densities higher than  $37 \text{ kg m}^{-3}$  in  $\sigma_2$ ) is measured by the SRT effect in the ocean interior, and it is largest in the Atlantic sector (Fig. 9b).

Strengthening and poleward shift of the westerlies in the faf-stress experiment produces strong cooling of the sSO (e.g.,

Fig. 9d). Cooling from convection in deep mixed layers intensifies across sectors (Figs. 9f, 10f, 11f, and 12f), even in the east Pacific sector; while the Ross OWP is confined to the west Pacific in the control run, it expands substantially in faf-stress (Figs. 3a,c). The SRT has a similar effect as in the control state, counterbalancing the cooling from surface boundary layer processes locally (i.e., in deep mixed layers) and spreading cold



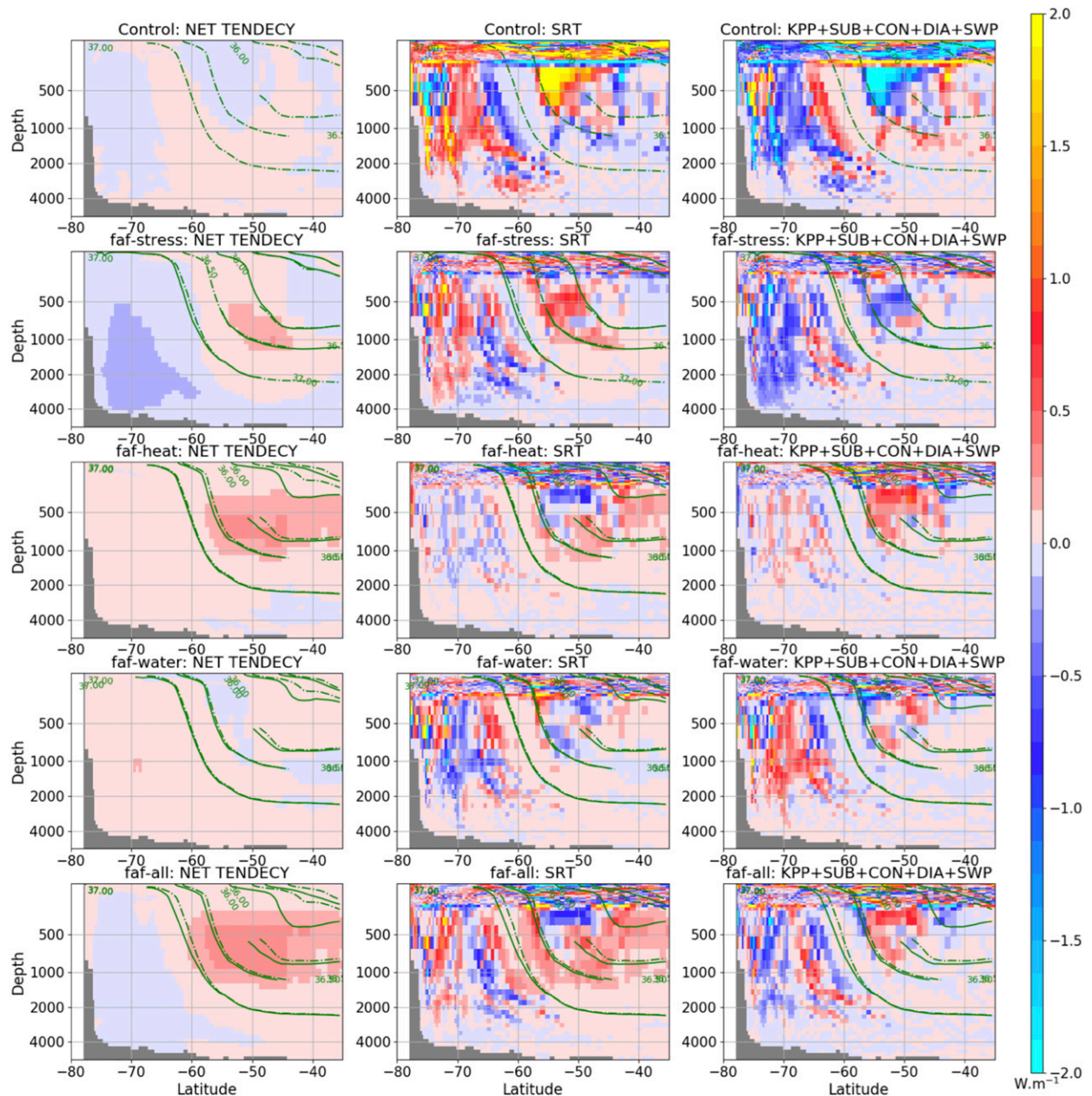


FIG. 10. As in Fig. 9, but for the west Pacific sector ( $137^{\circ}\text{E}$ – $130^{\circ}\text{W}$ ) of the Southern Ocean.

water equatorward of  $65^{\circ}\text{S}$  and below 2000 m (Figs. 9e, 12e, 10e, and 11e). In contrast with the control state, where most export of AABW occurs in the Atlantic sector (Fig. 9b), in faf-stress there is also strong northward bottom water transport in the Indian and east Pacific sectors (Figs. 12e and 11e). The advection of AABW via SRT in the ocean interior, however, is only weakly counterbalanced by DIA, which indicates that the diapycnal diffusion has a slower response to AABW formation than advective processes over the time scale of our experiments. The interpretation of the budget analyses presented here is supported by the

analyses of specific periods (e.g., increase or weakening of the OWPs; not shown).

The response to positive heat flux (faf-heat) and increased freshwater flux (faf-water) anomalies around the Southern Ocean is generally opposite to the changes from faf-stress (Figs. 9g,j). Both convection and SRT show reduced respective cooling and warming tendencies compared to the control state (Figs. 9b,c,h,i,k,l), meaning that dense water formation slows (Fig. 5a). The slowdown of convection is stronger in the Weddell Sea in faf-heat (Fig. 9i), while convection generally weakens also in the Ross Sea in faf-water (Figs. 9l and 10l).



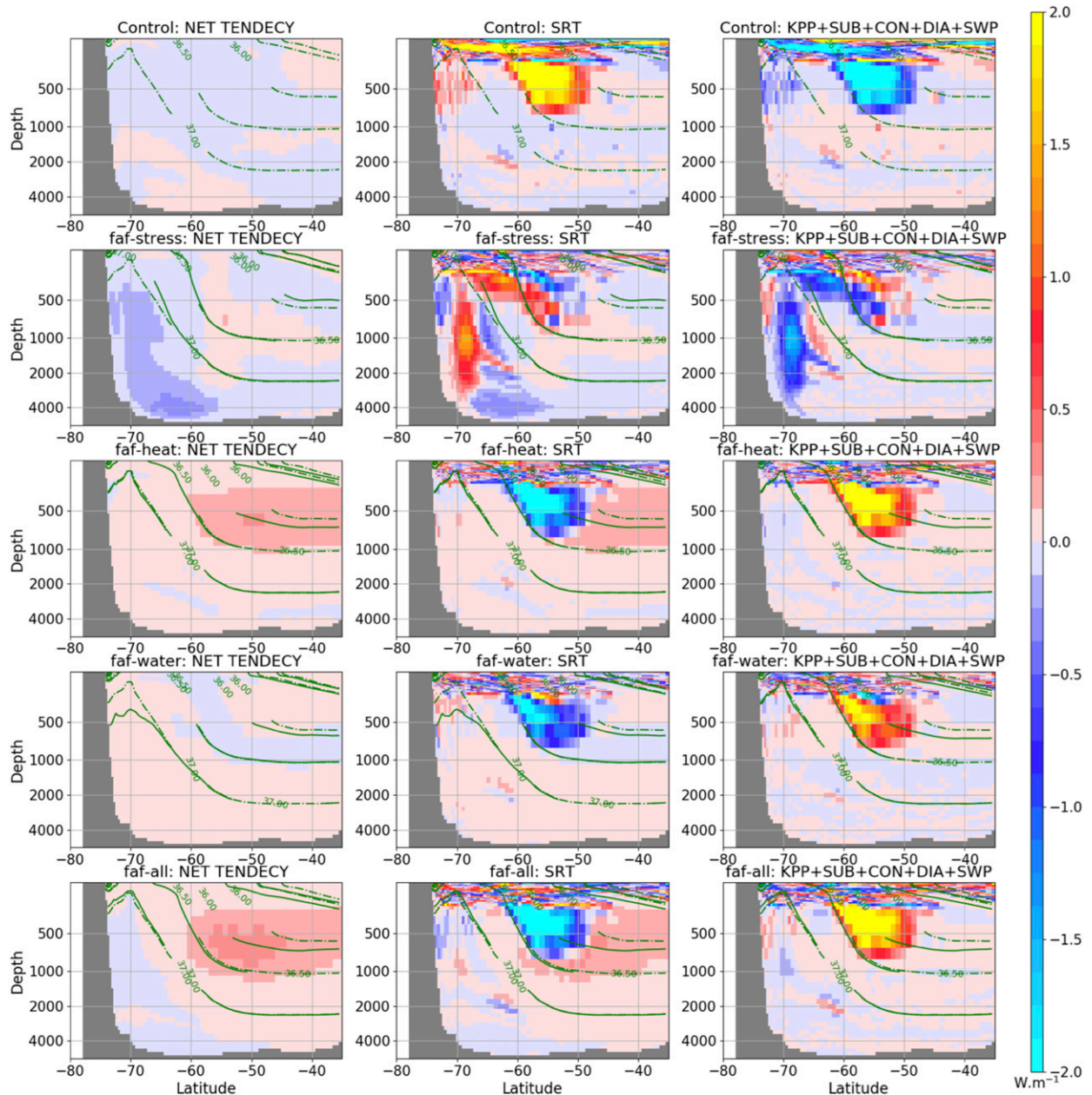


FIG. 11. As in Fig. 9, but for the east Pacific sector ( $130^{\circ}$ – $70^{\circ}$ W) of the Southern Ocean.

Below and poleward of the deep mixed layers, the SRT transfers warm anomalies along the ocean bottom toward lower latitudes. South of  $60^{\circ}$ S, the ocean response to faf-water and faf-heat is similar, with slightly larger response to SFWFp (Figs. 9h,k and 12h,k).

In faf-all (Figs. 9m, 10m, 11m, and 12m), the cooling response from faf-stress dominates the warming effect from faf-heat and faf-water (Fig. 2h). This response, however, is not constant over the simulation (Fig. 5). The cycles of intensification and reduction of the MOC transport (and expansion and contraction of the OWP) impact the heat budget analyses, with net cooling or warming dependent on time

intervals chosen to average budget diagnostics (not shown). The analyses shown in Figs. 9–12 are averages over the whole 80-yr simulation.

## 5. Discussion

Our ocean heat budget analyses explain quantitative changes in OHC, watermass properties, and MOC transport shown in section 3. OWPs, where a large fraction of AABW is formed in the model, expand due to wind perturbations (Figs. 3d,j), enhancing ocean surface heat loss (Fig. 8c). During OWP events, the ocean cools from the surface to the

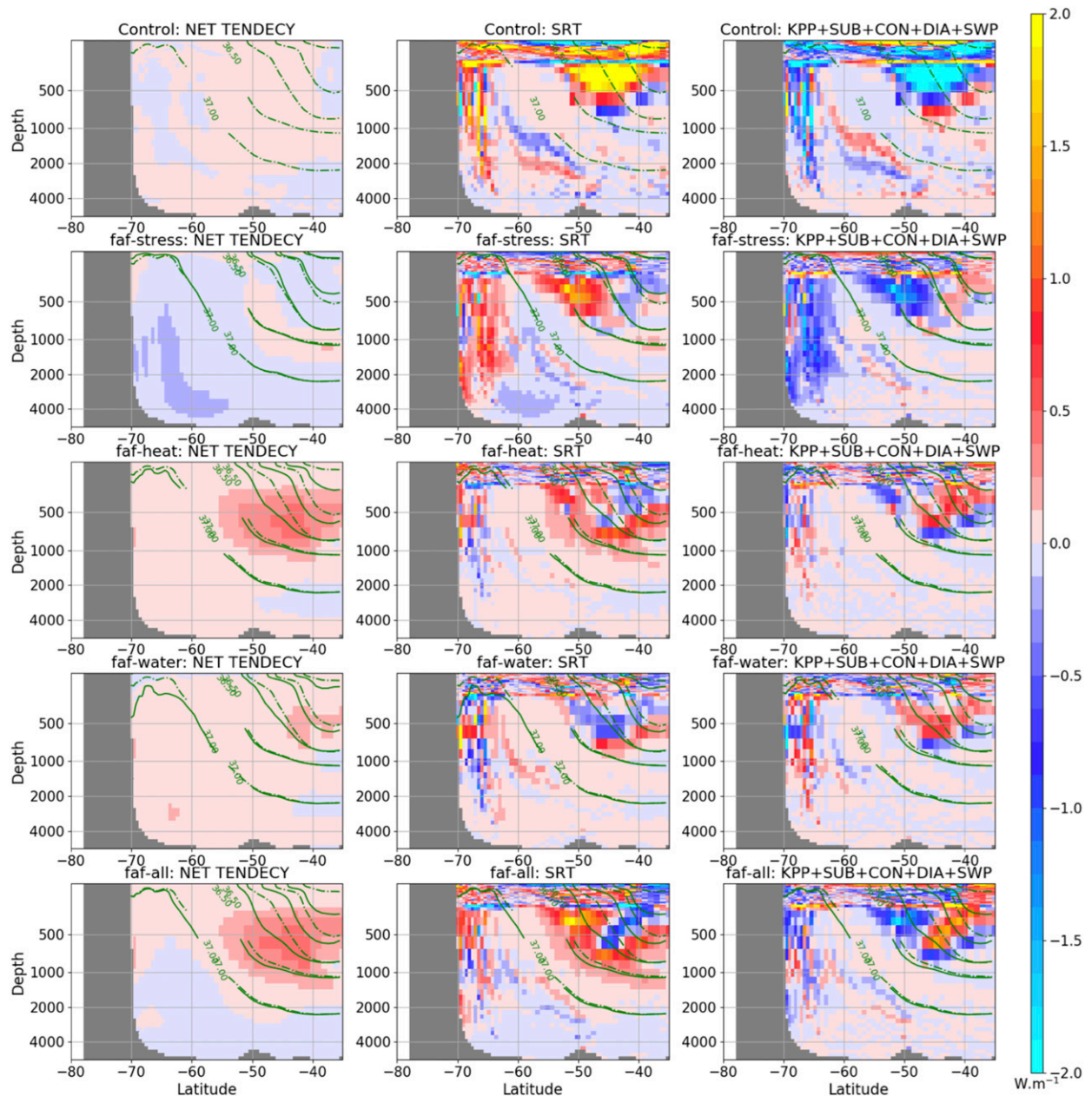


FIG. 12. As in Fig. 9, but for the Indian sector ( $20^{\circ}$ – $137^{\circ}$ E) of the Southern Ocean.

bottom (Figs. 6b,e and 9d), venting the middepth heat reservoir. Deep convection is driven by the intensification of mixing processes in the surface boundary layer (mostly due to convection and nonlocal KPP; e.g., Fig. 9f), enhancing AABW formation and the lower limb of the MOC (Fig. 5a). The watermass analysis shows that HSSW becomes saltier and WSBW/RSBW become colder, forming denser AABW (Fig. 4). In contrast, heat and freshwater perturbations reduce ice-free regions (Figs. 3f,h), surface heat loss (Figs. 8e,g), and the ocean processes associated with AABW formation (Figs. 9i,l).

The superresidual framework presented in Dias et al. (2020a) and applied to this budget analysis proves useful to identify where

and how AABW is formed and exported. Ocean cooling by surface boundary layer processes is locally balanced by warming due to the SRT, which also transfers AABW from its formation regions equatorward. In *faf-stress*, where AABW formation increases substantially, the export of AABW occurs in all sectors of the Southern Ocean (Figs. 9e, 10e, 11e, and 12e). In experiments where the AABW formation decreases (*faf-heat* and *faf-water*), the SRT drives warm anomalies in the ocean interior (equatorward of  $60^{\circ}$ S and below 2000 m), especially in the Atlantic sector where most AABW export occurs in the control state (Figs. 9h,k).

The physical mechanism by which wind perturbations drive enhanced deep open-ocean convection is as follows.

An intensification and southward shift of winds cause upwelling of warm and salty waters. Anomalous warm waters inhibit sea ice formation during winter (Figs. 7e,f), increasing the open water area and surface heat loss (Fig. 8c) and enhancing the physical processes associated with convective overturning. In contrast, positive anomalies of SHFp and SFWFp increase the sSO stratification (Figs. 6c,d,h,i) and expand the sea ice cover (Figs. 3f,h), consistent with prior results (Marsland and Wolff 2001; Lago and England 2019; Moorman et al. 2020). In summary, processes that enhance deep convection (e.g., strong winds and cold air temperature) lead to cooling (OHC decrease), and processes that stratify the ocean (positive heat and FW input), inhibit deep convection, and lead to a build-up of heat below the surface.

As the magnitude of individual flux perturbations comes directly from the CMIP5 ensemble mean, the quantification of the sSO response to changes in surface forcing has important implications for interpretation of climate change projections. The lower limb of the MOC results from the upwelling of CDW and sinking of denser AABW. In general, studies of CO<sub>2</sub>-perturbed climate have associated surface warming and/or freshening with decreases in convection and a slowdown in the abyssal MOC (Manabe et al. 1990; Gregory 2000; Bi 2002; Huang et al. 2003; de Lavergne et al. 2014; Exarchou et al. 2015). Moreover, studies that investigated the effect of wind changes (strengthening and southward migration of the westerlies) on ocean heat uptake and sea level have shown that cooling and sea level decreases occur near Antarctica (Bouttes et al. 2012; Frankcombe et al. 2013; Kuhlbrodt et al. 2015).

Although the strengthening of AABW formation and lower MOC due to southward shifting winds has been found in other studies (e.g., Kuhlbrodt et al. 2015), our finding that the strengthening due to wind perturbation dominates over the weakening of MOC by freshwater and heat flux perturbations is somewhat surprising. Observed trends in AABW composition over recent decades have revealed a warming and density reduction in the Atlantic and Pacific sectors (Coles et al. 1996; Johnson et al. 2007; Purkey and Johnson 2010), as well as freshening and density decrease in the Australian-Antarctic basin and the Weddell and Amundsen Seas (Rintoul 2007; Hellmer et al. 2011; Jullion et al. 2013; Bindoff and Hobbs 2013; Dotto et al. 2016). A similar response is seen in ACCESS-OM2 due to surface heat and freshwater perturbations, where OWPs and AABW formation decrease. The latest observations indicate that these trends may be currently stabilizing or even reversing (Abrahamsen et al. 2019; Silvano et al. 2020; Aoki et al. 2020). Analysis of CMIP5 models under increased radiative forcing shows an increase in AABW salinity and density (Sallée et al. 2013), although spread among models is large. Also analyzing CMIP5 models, Heuzé et al. (2015) found a warming trend in the Southern Ocean bottom temperature, but bottom salinity trends vary between models. In our results, cooling and increase of salinity and density of the AABW is a response to the decrease of sea ice during OWP events, allowing rates of surface heat loss at least twice as large as the control experiment (Figs. 8a,c), inducing strong deep convection that mixes CDW vertically and abruptly accelerates

the MOC. Notably, this is a fundamental mechanism of AABW formation in our model and many others (Heuzé et al. 2013; Mohrmann et al. 2021).

Dense watermasses (e.g., AABW, NADW) conserve their properties from the formation regions, and our results suggest that spread of projected AABW properties among CMIP models is linked with mechanisms of AABW formation. Models with AABW formation through OWP may respond to climate change just as ACCESS-OM2, causing OHC decrease through deep convection. In contrast, models without OWPs might respond differently to wind changes due to the sea ice coverage (Schulze and Pickard 2012)—if the effects from the heat and freshwater perturbation dominate, it would result in OHC increase. Mohrmann et al. (2021) found that half of 27 CMIP6 models form OWP, and a large spread in the AABW response has been found in previous CMIPs (Sallée et al. 2013; Heuzé et al. 2015).

Although formation of AABW via deep open-ocean convection has been observed in the past (Killworth 1983), it is a relatively rare phenomenon. The Weddell Polynya was observed during three consecutive winters between 1974 and 1976 (Zwally and Gloersen 1977; Carsey 1980; Gordon and Comiso 1988), and only in recent years (2016–17) a somewhat smaller OWP was observed in the vicinity of the Maud Rise (Campbell et al. 2019). Typically, AABW formation involves mixing of HSSW, a product of brine rejection by sea ice formation on the Antarctic continental shelf, and CDW flowing southward and upwelling in the Southern Ocean (Carmack and Foster 1975; Foster and Carmack 1976). This process is particularly strong in Antarctic coastal polynyas (e.g., Marsland et al. 2007; Tamura et al. 2008; Kusahara et al. 2017). Dense Ice Shelf Waters (ISW) formed by sub-ice-shelf melting may also contribute to AABW formation (Foldvik et al. 1985). These small-scale sub-ice-shelf processes need sufficient model resolution to resolve local flow variations over the continental shelf and in the ice shelf cavities, which are not well represented in global climate models (Heuzé et al. 2013; Mohrmann et al. 2021) and ocean reanalyses (Azaneu et al. 2014; Aguiar et al. 2017).

Given that many climate/ocean models form AABW through deep open-ocean convection rather than over the continental shelf, the real ocean, with less open-ocean convection and more coastal convection, would probably respond differently to the FAFMIP perturbations. Nevertheless, the overall message of our study remains robust: processes that increase convection and AABW formation will cool the deep ocean, independent of where they occur; while processes that increase stratification will reduce AABW formation and venting of heat from CDW. The Weddell and Ross OWPs show important differences in response to surface perturbations. Wind changes induced different timing of the OWP events, and the eastward expansion of the Ross OWP causes active convection in the east Pacific sector (where no convection occurs in the control state). The Ross OWP is not affected by the heat flux perturbation, but both OWPs retreat due to FWF perturbation. Studies based on climate models have shown different responses of bottom water to forcing perturbations. De Lavergne et al. (2014) suggested the cessation of deep convection in both convective and nonconvective models under RCP8.5 simulations. Analyses of CMIP5 models under RCP4.5



and RCP8.5 scenarios suggest increases in salinity and density of bottom waters (Sallée et al. 2013; Meijers 2014)—although with a large spread in the AABW response (Heuzé et al. 2015). High-resolution models can better represent the small-scale physics of shelf processes, mesoscale eddies, and overflow of dense waters, which affect the ocean stratification, heat transport, and OWP (Dufour et al. 2017). Therefore, high-resolution models might respond differently to surface perturbations than coarse models. CMIP5/CMIP6 models and the ACCESS-OM2 do not include ice shelf/sheet melting, and hence underestimate the impact of the freshwater fluxes on the vertical stratification and deep convection (Kjellsson et al. 2015; Stössel et al. 2015). In particular, Antarctic meltwater from drifting icebergs and basal melting can strongly reduce AABW formation (Kusahara and Hasumi 2013; Lago and England 2019).

Importantly, these results are based on ocean-only simulations and might differ from the fully coupled model response. Although ACCESS-OM2 is driven by a prescribed atmosphere (JRA55-do), it can also induce ocean–atmosphere feedbacks due to the impact of the ocean circulation (and associated SST) on the surface fluxes, just like AOGCMs (Gregory et al. 2016) and unlike the ocean-only FAFMIP simulations in Todd et al. (2020). The main difference between our bulk formula setup and AOGCMs is that the atmosphere can freely evolve in the latter, which might have impacts on the realism of ocean–atmosphere feedbacks. OWPs tend to increase the surface air temperature (Kaufman et al. 2020), which can affect the duration and intensity of OWP events. While ocean–atmosphere feedbacks are known to be relevant in the North Atlantic (Gregory et al. 2016), our results show that they can also play a role in the Southern Ocean during large convective events (Figs. 8c,i). Similar mechanisms of OWP evolution involving heat build-up and release through deep convection, as found in this study, have also been previously suggested for AOGCMs (Martin et al. 2013; Behrens et al. 2016; Latif et al. 2017; Reintges et al. 2017).

## 6. Conclusions

This study presents detailed analyses of the subpolar Southern Ocean response to perturbations in surface forcing. Using OGCM simulations driven by FAFMIP flux anomalies derived from an ensemble of CMIP5 models under a 2xCO<sub>2</sub> scenario, results reveal that the sSO is dominated by the response to wind forcing perturbations. Wind perturbations reduce sea ice growth during winter due to upwelling of warm deep waters, which trigger OWP events in the Weddell and Ross Seas, allowing strong ocean–atmosphere heat exchange and deep ocean convection. The heat and freshwater perturbations have opposite effect to wind perturbations, tending to increase vertical stratification and sea ice growth, but only partially compensating wind effects. The response is not exactly linear, as the Weddell and Ross OWP exhibit large interdecadal variability, reflecting the build-up and depletion of the middepth heat reservoir.

These findings are useful for interpretation of climate change projections. The OHC decrease near Antarctica leads to seawater contraction and local sea level decrease, which are often seen in climate model projections (Gregory et al. 2016)

and might indicate a future increase of OWP events. The large spread of sea level projections in the Southern Ocean (e.g., Kuhlbrodt and Gregory 2012) can be associated with a distinct response of convective and nonconvective models to surface forcing perturbations in the sSO (Mohrman et al. 2021). As coarse horizontal resolution climate models have limited representation of shelf processes of AABW formation, and high-resolution models are currently not viable for centennial/millennial simulations required for climate projections, this uncertainty might represent a major limitation on the current understanding of the ocean's response to climate change.

*Acknowledgments.* This work was supported by the Australian Research Council (ARC) Discovery Grant DP160103130, ARC Centre of Excellence for Climate Extremes (CE170100023), and the National Computational Infrastructure through the National Computational Merit Allocation Scheme. FBD and AS were supported by a Tasmanian Graduate Research Scholarship and CSIRO-UTAS Quantitative Marine Science top-up. FBD and PU were supported by the Academy of Finland (Project 322432). RF, SJM, and SRR were supported by the Earth Systems and Climate Change Hub of the Australian Government's National Environmental Science Program. SRR was jointly supported by the Australian Antarctic Program Partnership and by the Centre for Southern Hemisphere Ocean Research, a partnership between CSIRO and the Qingdao National Laboratory for Marine Science and Technology (QNLN). CMD was supported by an ARC Future Fellowship FT130101532 and by the Natural Environment Research Council NE/P019293/1. MMM was supported by the Brazilian Research Council CNPq research grant 306896/2015-0. We are thankful for the support from the Consortium for Ocean–Sea-Ice Modelling in Australia (COSIMA) and to Adam Blaker for useful discussion on the experiment design. We appreciated the constructive comments from the reviewers that helped to improve the manuscript.

## REFERENCES

- Abrahamsen, E. P., and Coauthors, 2019: Stabilization of dense Antarctic water supply to the Atlantic Ocean overturning circulation. *Nat. Climate Change*, **9**, 742–746, <https://doi.org/10.1038/s41558-019-0561-2>.
- Aguiar, W., M. M. Mata, and R. Kerr, 2017: On deep convection events and Antarctic Bottom Water formation in ocean re-analysis products. *Ocean Sci.*, **13**, 851–872, <https://doi.org/10.5194/os-13-851-2017>.
- Aoki, S., K. Yamazaki, D. Hirano, K. Katsumata, K. Shimada, Y. Kitade, H. Sasaki, and H. Murase, 2020: Reversal of freshening trend of Antarctic Bottom Water in the Australian–Antarctic Basin during 2010s. *Sci. Rep.*, **10**, 14415, <https://doi.org/10.1038/s41598-020-71290-6>.
- Azaneu, M., R. Kerr, and M. M. Mata, 2014: Assessment of the representation of Antarctic Bottom Water properties in the ECCO2 reanalysis. *Ocean Sci.*, **10**, 923–946, <https://doi.org/10.5194/os-10-923-2014>.
- Baines, P. G., and S. Condie, 1985: *Observations and Modelling of Antarctic Downslope Flows: A Review*. Amer. Geophys. Union, 29–49.
- Banks, H. T., and J. M. Gregory, 2006: Mechanisms of ocean heat uptake in a coupled climate model and the implications for

- tracer based predictions of ocean heat uptake. *Geophys. Res. Lett.*, **33**, L07608, <https://doi.org/10.1029/2005GL025352>.
- Behrens, E., G. Rickard, O. Morgenstern, T. Martin, A. Osprey, and M. Joshi, 2016: Southern Ocean deep convection in global climate models: A driver for variability of subpolar gyres and Drake Passage transport on decadal timescales. *J. Geophys. Res. Oceans*, **121**, 3905–3925, <https://doi.org/10.1002/2015JC011286>.
- Bi, D., 2002: Transient and long-term behaviour of the World Ocean under global warming. Ph.D. thesis, University of Tasmania, 301 pp.
- Bindoff, N. L., and W. R. Hobbs, 2013: Oceanography: Deep ocean freshening. *Nat. Climate Change*, **3**, 864–865, <https://doi.org/10.1038/nclimate2014>.
- Bouttes, N., and J. M. Gregory, 2014: Attribution of the spatial pattern of CO<sub>2</sub>-forced sea level change to ocean surface flux changes. *Environ. Res. Lett.*, **9**, 034004, <https://doi.org/10.1088/1748-9326/9/3/034004>.
- , —, T. Kuhlbrodt, and T. Suzuki, 2012: The effect of windstress change on future sea level change in the Southern Ocean. *Geophys. Res. Lett.*, **39**, 1–6, <https://doi.org/10.1029/2012GL054207>.
- Campbell, E. C., E. A. Wilson, K. Moore, S. C. Riser, C. E. Brayton, M. R. Mazloff, and L. D. Talley, 2019: Antarctic offshore polynyas linked to Southern Hemisphere climate anomalies. *Nature*, **570**, 319–325, <https://doi.org/10.1038/s41586-019-1294-0>.
- Carmack, E. C., and T. D. Foster, 1975: On the flow of water out of the Weddell Sea. *Deep-Sea Res. Oceanogr. Abstr.*, **22**, 711–724, [https://doi.org/10.1016/0011-7471\(75\)90077-7](https://doi.org/10.1016/0011-7471(75)90077-7).
- Carsey, F. D., 1980: Microwave observation of the Weddell polynya. *Mon. Wea. Rev.*, **108**, 2032–2044, [https://doi.org/10.1175/1520-0493\(1980\)108<2032:MOOTWP>2.0.CO;2](https://doi.org/10.1175/1520-0493(1980)108<2032:MOOTWP>2.0.CO;2).
- Cheon, W. G., and A. L. Gordon, 2019: Open-ocean polynyas and deep convection in the Southern Ocean. *Sci. Rep.*, **9**, 6935, <https://doi.org/10.1038/s41598-019-43466-2>.
- Church, J., and Coauthors, 2011: Revisiting the Earth's sea-level and energy budgets from 1961 to 2008. *Geophys. Res. Lett.*, **38**, L18601, <https://doi.org/10.1029/2011GL048794>.
- , D. Monselesan, J. M. Gregory, and B. Marzeion, 2013: Evaluating the ability of process based models to project sea-level change. *Environ. Res. Lett.*, **8**, 014051, <https://doi.org/10.1088/1748-9326/8/1/014051>.
- Coles, V. J., M. S. McCartney, D. B. Olson, and W. M. Smethie, 1996: Changes in Antarctic Bottom Water properties in the western South Atlantic in the late 1980s. *J. Geophys. Res. Oceans*, **101**, 8957–8970, <https://doi.org/10.1029/95JC03721>.
- Comiso, J. C., and A. L. Gordon, 1987: Recurring polynyas over the Cosmonaut Sea and the Maud Rise. *J. Geophys. Res. Oceans*, **92**, 2819–2833, <https://doi.org/10.1029/JC092iC03p02819>.
- , R. Kwok, S. Martin, and A. L. Gordon, 2011: Variability and trends in sea ice extent and ice production in the Ross Sea. *J. Geophys. Res.*, **116**, C04021, <https://doi.org/10.1029/2010JC006391>.
- Couldrey, M. P., and Coauthors, 2021: What causes the spread of model projections of ocean dynamic sea-level change in response to greenhouse gas forcing? *Climate Dyn.*, **56**, 155–187, <https://doi.org/10.1007/s00382-020-05471-4>.
- Danabasoglu, G., and Coauthors, 2014: North Atlantic simulations in coordinated ocean-ice reference experiments phase II (CORE-II). Part I: Mean states. *Ocean Modell.*, **73**, 76–107, <https://doi.org/10.1016/j.ocemod.2013.10.005>.
- de Lavergne, C., J. B. Palter, E. D. Galbraith, R. Bernardello, and I. Marinov, 2014: Cessation of deep convection in the open Southern Ocean under anthropogenic climate change. *Nat. Climate Change*, **4**, 278–282, <https://doi.org/10.1038/nclimate2132>.
- Dias, F. B., C. M. Domingues, S. J. Marsland, S. M. Griffies, S. R. Rintoul, R. Matear, and R. Fiedler, 2020a: On the superposition of mean advective and eddy-induced transports in global ocean heat and salt budgets. *J. Climate*, **33**, 1121–1140, <https://doi.org/10.1175/JCLI-D-19-0418.1>.
- , and Coauthors, 2020b: Ocean heat storage in response to changing ocean circulation processes. *J. Climate*, **33**, 9065–9082, <https://doi.org/10.1175/JCLI-D-19-1016.1>.
- Dotto, T. S., R. Kerr, M. M. Mata, and C. A. E. Garcia, 2016: Multidecadal freshening and lightening in the deep waters of the Bransfield Strait, Antarctica. *J. Geophys. Res. Oceans*, **121**, 3741–3756, <https://doi.org/10.1002/2015JC011228>.
- Downes, S. M., and Coauthors, 2015: An assessment of Southern Ocean water masses and sea ice during 1988–2007 in a suite of interannual CORE-II simulations. *Ocean Modell.*, **94**, 67–94, <https://doi.org/10.1016/j.ocemod.2015.07.022>.
- Drucker, R., S. Martin, and R. Kwok, 2011: Sea ice production and export from coastal polynyas in the Weddell and Ross Seas. *Geophys. Res. Lett.*, **38**, L17502, <https://doi.org/10.1029/2011GL048668>.
- Dufour, C. O., A. K. Morrison, S. M. Griffies, I. Frenger, H. Zanowski, and M. Winton, 2017: Preconditioning of the Weddell Sea polynya by the ocean mesoscale and dense water overflows. *J. Climate*, **30**, 7719–7737, <https://doi.org/10.1175/JCLI-D-16-0586.1>.
- Durack, P. J., S. E. Wijffels, and P. J. Gleckler, 2014: Long-term sea-level change revisited: The role of salinity. *Environ. Res. Lett.*, **9**, 114017, <https://doi.org/10.1088/1748-9326/9/11/114017>.
- Exarchou, E., T. Kuhlbrodt, J. M. Gregory, and R. S. Smith, 2015: Ocean heat uptake processes: A model intercomparison. *J. Climate*, **28**, 887–908, <https://doi.org/10.1175/JCLI-D-14-00235.1>.
- Fahrbach, E., M. Hoppema, G. Rohardt, O. Boebel, O. Klatt, and A. Wisotzki, 2011: Warming of deep and abyssal water masses along the Greenwich meridian on decadal time scales: The Weddell Gyre as a heat buffer. *Deep-Sea Res. II*, **58**, 2509–2523, <https://doi.org/10.1016/j.dsr2.2011.06.007>.
- Ferrari, R., A. Mashayek, T. J. McDougall, M. Nikurashin, and J.-M. Campin, 2016: Turning ocean mixing upside down. *J. Phys. Oceanogr.*, **46**, 2239–2261, <https://doi.org/10.1175/JPO-D-15-0244.1>.
- Foldvik, A., T. Gammelsrød, and T. Tørresen, 1985: Circulation and water masses on the southern Weddell Sea shelf. *Oceanology of the Antarctic Continental Shelf*. S. S. Jacobs, Ed., Vol. 43, Amer. Geophys. Union, 5–20.
- Foster, T. D., and E. C. Carmack, 1976: Frontal zone mixing and Antarctic bottom water formation in the southern Weddell Sea. *Deep-Sea Res. Oceanogr. Abstr.*, **23**, 301–317, [https://doi.org/10.1016/0011-7471\(76\)90872-X](https://doi.org/10.1016/0011-7471(76)90872-X).
- Frankcombe, L. M., P. Spence, A. M. Hogg, M. H. England, and S. M. Griffies, 2013: Sea level changes forced by Southern Ocean winds. *Geophys. Res. Lett.*, **40**, 5710–5715, <https://doi.org/10.1002/2013GL058104>.
- Garuba, O. A., and B. A. Klinger, 2016: Ocean heat uptake and interbasin transport of the passive and redistributive components of surface heating. *J. Climate*, **29**, 7507–7527, <https://doi.org/10.1175/JCLI-D-16-0138.1>.
- Gordon, A. L., and J. C. Comiso, 1988: Polynyas in the Southern Ocean the global heat engine that couples the ocean and the atmosphere. *Sci. Amer.*, **258**, 90–97, <https://doi.org/10.1038/scientificamerican0688-90>.
- Gregory, J. M., 2000: Vertical heat transports in the ocean and their effect on time-dependent climate change. *Climate Dyn.*, **16**, 501–515, <https://doi.org/10.1007/s003820000059>.

- , and Coauthors, 2016: The Flux-Anomaly-Forced Model Intercomparison Project (FAFMIP) contribution to CMIP6: Investigation of sea-level and ocean climate change in response to CO<sub>2</sub> forcing. *Geosci. Model Dev.*, **9**, 3993–4017, <https://doi.org/10.5194/gmd-9-3993-2016>.
- Griffies, S. M., and R. J. Greatbatch, 2012: Physical processes that impact the evolution of global mean sea level in ocean climate models. *Ocean Modell.*, **51**, 37–72, <https://doi.org/10.1016/j.ocemod.2012.04.003>.
- , and Coauthors, 2015: Impacts on ocean heat from transient mesoscale eddies in a hierarchy of climate models. *J. Climate*, **28**, 952–977, <https://doi.org/10.1175/JCLI-D-14-00353.1>.
- Hellmer, H. H., O. Huhn, D. Gomis, and R. Timmermann, 2011: On the freshening of the northwestern Weddell Sea continental shelf. *Ocean Sci.*, **7**, 305–316, <https://doi.org/10.5194/os-7-305-2011>.
- Heuzé, C., K. J. Heywood, D. P. Stevens, and J. K. Ridley, 2013: Southern Ocean bottom water characteristics in CMIP5 models. *Geophys. Res. Lett.*, **40**, 1409–1414, <https://doi.org/10.1002/grl.50287>.
- , —, —, and —, 2015: Changes in global ocean bottom properties and volume transports in CMIP5 models under climate change scenarios. *J. Climate*, **28**, 2917–2944, <https://doi.org/10.1175/JCLI-D-14-00381.1>.
- Hobbs, W., M. D. Palmer, and D. Monselesan, 2016: An energy conservation analysis of ocean drift in the CMIP5 global coupled models. *J. Climate*, **29**, 1639–1653, <https://doi.org/10.1175/JCLI-D-15-0477.1>.
- Holmes, R. M., C. de Lavergne, T. J. McDougall, R. M. Holmes, C. de Lavergne, and T. J. McDougall, 2018: Ridges, seamounts, troughs, and bowls: Topographic control of the dia-neutral circulation in the Abyssal Ocean. *J. Phys. Oceanogr.*, **48**, 861–882, <https://doi.org/10.1175/JPO-D-17-0141.1>.
- Huang, B., P. H. Stone, A. P. Sokolov, and I. V. Kamenkovich, 2003: The deep-ocean heat uptake in transient climate change. *J. Climate*, **16**, 1352–1363, <https://doi.org/10.1175/1520-0442-16.9.1352>.
- Hunke, E. C., W. H. Lipscomb, A. K. Turner, N. Jeffery, and S. Elliott, 2013: CICE: The Los Alamos Sea Ice Model documentation and software user's manual. Tech Rep. LA-CC-06-012, 115 pp.
- Johnson, G. C., 2008: Quantifying Antarctic Bottom Water and North Atlantic Deep Water volumes. *J. Geophys. Res. Oceans*, **113**, C05027, <https://doi.org/10.1029/2007JC004477>.
- , S. Mecking, B. M. Sloyan, and S. E. Wijffels, 2007: Recent bottom water warming in the Pacific Ocean. *J. Climate*, **20**, 5365–5375, <https://doi.org/10.1175/2007JCLI1879.1>.
- Jullion, L., A. C. Garabato, M. P. Meredith, P. R. Holland, P. Courtis, and B. A. King, 2013: Decadal freshening of the Antarctic Bottom Water exported from the Weddell Sea. *J. Climate*, **26**, 8111–8125, <https://doi.org/10.1175/JCLI-D-12-00765.1>.
- Kaufman, Z. S., N. Feldl, W. Weijer, and M. Veneziani, 2020: Causal interactions between Southern Ocean polynyas and high-latitude atmosphere–ocean variability. *J. Climate*, **33**, 4891–4905, <https://doi.org/10.1175/JCLI-D-19-0525.1>.
- Kerr, R., M. M. Mata, and C. A. E. Garcia, 2009: On the temporal variability of the Weddell Sea deep water masses. *Antarct. Sci.*, **21**, 383–400, <https://doi.org/10.1017/S0954102009001990>.
- , K. J. Heywood, M. M. Mata, and C. A. Garcia, 2012: On the outflow of dense water from the Weddell and Ross Seas in OCCAM model. *Ocean Sci.*, **8**, 369–388, <https://doi.org/10.5194/os-8-369-2012>.
- , T. S. Dotto, M. M. Mata, and H. H. Hellmer, 2018: Three decades of deep water mass investigation in the Weddell Sea (1984–2014): Temporal variability and changes. *Deep-Sea Res. II*, **149**, 70–83, <https://doi.org/10.1016/j.dsr2.2017.12.002>.
- Killworth, P. D., 1983: Deep convection in the World Ocean. *Rev. Geophys.*, **21**, 1–26, <https://doi.org/10.1029/RG021i001p00001>.
- Kiss, A. E., and Coauthors, 2020: ACCESS-OM2 v1.0: A global ocean–sea ice model at three resolutions. *Geosci. Model Dev.*, **13**, 401–442, <https://doi.org/10.5194/gmd-13-401-2020>.
- Kjellsson, J., and Coauthors, 2015: Model sensitivity of the Weddell and Ross Seas, Antarctica, to vertical mixing and freshwater forcing. *Ocean Modell.*, **94**, 141–152, <https://doi.org/10.1016/j.ocemod.2015.08.003>.
- Kuhlbrodt, T., and J. M. Gregory, 2012: Ocean heat uptake and its consequences for the magnitude of sea level rise and climate change. *Geophys. Res. Lett.*, **39**, L18608, <https://doi.org/10.1029/2012GL052952>.
- , A. Griesel, M. Montoya, A. Levermann, M. Hofmann, and S. Rahmstorf, 2007: On the driving processes of the Atlantic meridional overturning circulation. *Rev. Geophys.*, **45**, RG2001, <https://doi.org/10.1029/2004RG000166.1>.
- , J. M. Gregory, and L. C. Shaffrey, 2015: A process-based analysis of ocean heat uptake in an AOGCM with an eddy-permitting ocean component. *Climate Dyn.*, **45**, 3205–3226, <https://doi.org/10.1007/s00382-015-2534-0>.
- Kusahara, K., and H. Hasumi, 2013: Modeling Antarctic ice shelf responses to future climate changes and impacts on the ocean. *J. Geophys. Res. Oceans*, **118**, 2454–2475, <https://doi.org/10.1002/jgrc.20166>.
- , G. D. Williams, T. Tamura, R. Massom, and H. Hasumi, 2017: Dense shelf water spreading from Antarctic coastal polynyas to the deep Southern Ocean: A regional circumpolar model study. *J. Geophys. Res. Oceans*, **122**, 6238–6253, <https://doi.org/10.1002/2017JC012911>.
- Lago, V., and M. H. England, 2019: Projected slowdown of Antarctic bottom water formation in response to amplified meltwater contributions. *J. Climate*, **32**, 6319–6335, <https://doi.org/10.1175/JCLI-D-18-0622.1>.
- Large, W. G., J. C. McWilliams, and S. C. Doney, 1994: Oceanic vertical mixing: A review and a model with a nonlocal boundary-layer parameterization. *Rev. Geophys.*, **32**, 363–403, <https://doi.org/10.1029/94RG01872>.
- Latif, M., T. Martin, A. Reintges, and W. Park, 2017: Southern Ocean decadal variability and predictability. *Curr. Climate Change Rep.*, **3**, 163–173, <https://doi.org/10.1007/s40641-017-0068-8>.
- Locarnini, R. A., and Coauthors, 2018: *Temperature*. Vol. I, *World Ocean Atlas 2018*, NOAA Atlas NESDIS 81, 52 pp.
- Manabe, S., K. Bryan, and M. J. Spelman, 1990: Transient response of a global ocean–atmosphere model to a doubling of atmospheric carbon dioxide. *J. Phys. Oceanogr.*, **20**, 722–749, [https://doi.org/10.1175/1520-0485\(1990\)020<0722:TROAGO>2.0.CO;2](https://doi.org/10.1175/1520-0485(1990)020<0722:TROAGO>2.0.CO;2).
- Marsland, S. J., and J.-O. Wolff, 2001: On the sensitivity of Southern Ocean sea ice to the surface freshwater flux: A model study. *J. Geophys. Res.*, **106**, 2723–2741, <https://doi.org/10.1029/2000JC900086>.
- , J. A. Church, N. L. Bindoff, and G. D. Williams, 2007: Antarctic coastal polynya response to climate change. *J. Geophys. Res.*, **112**, C07009, <https://doi.org/10.1029/2005JC003291>.
- Martin, T., W. Park, and M. Latif, 2013: Multi-centennial variability controlled by Southern Ocean convection in the Kiel Climate Model. *Climate Dyn.*, **40**, 2005–2022, <https://doi.org/10.1007/s00382-012-1586-7>.
- McDougall, T. J., and R. Ferrari, 2016: Abyssal upwelling and downwelling driven by near-boundary mixing. *J. Phys. Oceanogr.*, **47**, 261–283, <https://doi.org/10.1175/JPO-D-16-0082.1>.



- Meijers, A. J. S., 2014: The Southern Ocean in the Coupled Model Intercomparison Project phase 5. *Philos. Trans. Roy. Soc. London*, **A372**, 20130296, <https://doi.org/10.1098/rsta.2013.0296>.
- Mohrmann, M., C. Heuzé, and S. Swart, 2021: Southern Ocean polynyas in CMIP6 models. *Cryosphere*, **15**, 4281–4313, <https://doi.org/10.5194/tc-15-4281-2021>.
- Moorman, R., A. K. Morrison, and A. McC. Hogg, 2020: Thermal responses to Antarctic Ice shelf melt in an eddy-rich global ocean–sea ice model. *J. Climate*, **33**, 6599–6620, <https://doi.org/10.1175/JCLI-D-19-0846.1>.
- Munk, W. H., 1966: Abyssal recipes. *Deep-Sea Res.*, **13**, 707–730, [https://doi.org/10.1016/0011-7471\(66\)90602-4Get](https://doi.org/10.1016/0011-7471(66)90602-4Get).
- Naughten, K. A., K. J. Meissner, B. K. Galton-Fenzi, M. H. England, R. Timmermann, and H. H. Hellmer, 2018: Future projections of Antarctic ice shelf melting based on cmip5 scenarios. *J. Climate*, **31**, 5243–5261, <https://doi.org/10.1175/JCLI-D-17-0854.1>.
- Nowicki, S. M. J., and Coauthors, 2016: Ice Sheet Model Intercomparison Project (ISMIP6) contribution to CMIP6. *Geosci. Model Dev.*, **9**, 4521–4545, <https://doi.org/10.5194/gmd-9-4521-2016>.
- Ohshima, K. I., and Coauthors, 2013: Antarctic Bottom Water production by intense sea-ice formation in the Cape Darnley polynya. *Nat. Geosci.*, **6**, 235–240, <https://doi.org/10.1038/ngeo1738>.
- Oppenheimer, M., and Coauthors, 2019: Sea level rise and implications for low-lying islands, coasts and communities. *IPCC Special Report on the Ocean and Cryosphere in a Changing Climate*, H.-O. Pörtner et al., Eds., <https://www.ipcc.ch/srocc/chapter/chapter-4-sea-level-rise-and-implications-for-low-lying-islands-coasts-and-communities/>.
- Orsi, A. H., G. C. Johnson, and J. L. Bullister, 1999: Circulation, mixing and production of Antarctic Bottom Water. *Prog. Oceanogr.*, **43**, 55–109, [https://doi.org/10.1016/S0079-6611\(99\)00004-X](https://doi.org/10.1016/S0079-6611(99)00004-X).
- Palter, J. B., S. M. Griffies, B. L. Samuels, E. D. Galbraith, A. Gnanadesikan, and A. Klocker, 2013: The deep ocean buoyancy budget and its temporal variability. *J. Climate*, **27**, 551–573, <https://doi.org/10.1175/JCLI-D-13-00016.1>.
- Purkey, S. G., and G. C. Johnson, 2010: Warming of global abyssal and deep Southern Ocean waters between the 1990s and 2000s: Contributions to global heat and sea level rise budgets. *J. Climate*, **23**, 6336–6351, <https://doi.org/10.1175/2010JCLI3682.1>.
- , and —, 2013: Antarctic Bottom Water warming and freshening: Contributions to sea level rise, ocean freshwater budgets, and global heat gain. *J. Climate*, **26**, 6105–6122, <https://doi.org/10.1175/JCLI-D-12-00834.1>.
- Reintges, A., T. Martin, M. Latif, and W. Park, 2017: Physical controls of Southern Ocean deep-convection variability in CMIP5 models and the Kiel Climate Model. *Geophys. Res. Lett.*, **44**, 6951–6958, <https://doi.org/10.1002/2017GL074087>.
- Rintoul, S. R., 2007: Rapid freshening of Antarctic Bottom Water formed in the Indian and Pacific Oceans. *Geophys. Res. Lett.*, **34**, 1–5, <https://doi.org/10.1029/2006GL028550>.
- Saenko, O. A., J. M. Gregory, S. M. Griffies, M. P. Couldrey, and F. B. Dias, 2021: Contribution of ocean physics and dynamics at different scales to heat uptake in low-resolution AOGCMs. *J. Climate*, **34**, 2017–2035, <https://doi.org/10.1175/JCLI-D-20-0652.1>.
- Sallée, J., E. Shuckburgh, N. Bruneau, A. J. S. Meijers, T. J. Bracegirdle, Z. Wang, and T. Roy, 2013: Assessment of Southern Ocean water mass circulation and characteristics in CMIP5 models: Historical bias and forcing response. *J. Geophys. Res. Oceans*, **118**, 1830–1844, <https://doi.org/10.1002/jgrc.20135>.
- Savita, A., J. D. Zika, C. M. Domingues, S. J. Marsland, G. D. Evans, F. B. Dias, R. M. Holmes, and A. M. Hogg, 2021: Super residual circulation: A new perspective on ocean vertical heat transport. *J. Phys. Oceanogr.*, **51**, 2443–2462, <https://doi.org/10.1175/JPO-D-21-0008.1>.
- Schulze, L. M., and R. S. Pickard, 2012: Seasonal variation of upwelling in the Alaskan Beaufort Sea: Impact of sea ice cover. *J. Geophys. Res. Oceans*, **117**, 1978–2012, <https://doi.org/10.1029/2012JC007985>.
- Sen Gupta, A., L. C. Muir, J. N. Brown, S. J. Phipps, P. J. Durack, D. Monselesan, and S. E. Wijffels, 2013: Climate drift in the CMIP3 models. *J. Climate*, **25**, 4621–4640, <https://doi.org/10.1175/JCLI-D-11-00312.1>.
- Silvano, A., and Coauthors, 2020: Recent recovery of Antarctic Bottom Water formation in the Ross Sea driven by climate anomalies. *Nat. Geosci.*, **13**, 780–786, <https://doi.org/10.1038/s41561-020-00655-3>.
- Stewart, K. D., W. Kim, S. Urakawa, A. M. Hogg, S. Yeager, H. Tsujino, H. Nakano, and A. E. Kiss, 2020: JRA55-do-based repeat year forcing datasets for driving ocean–sea-ice models. *Ocean Modell.*, **147**, 147, <https://doi.org/10.1016/j.ocemod.2019.101557>.
- Stommel, H., and A. B. Arons, 1960: On the abyssal circulation of the world ocean—II. An idealized model of the circulation pattern and amplitude in oceanic basins. *Deep-Sea Res.*, **6**, 217–218, [https://doi.org/10.1016/0146-6313\(59\)90075-9](https://doi.org/10.1016/0146-6313(59)90075-9).
- Stössel, A., D. Notz, F. A. Haumann, H. Haak, J. JungCLAUS, and U. Mikolajewicz, 2015: Controlling high-latitude Southern Ocean convection in climate models. *Ocean Modell.*, **86**, 58–75, <https://doi.org/10.1016/j.ocemod.2014.11.008>.
- Tamura, T., K. I. Ohshima, and S. Nihashi, 2008: Mapping of sea ice production for Antarctic coastal polynyas. *Geophys. Res. Lett.*, **35**, L07606, <https://doi.org/10.1029/2007GL032903>.
- , —, —, and H. Hasumi, 2011: Estimation of surface heat/salt fluxes associated with sea ice growth/melt in the Southern Ocean. *Sci. Online Lett. Atmos.*, **7**, 17–20, <https://doi.org/10.2151/sola.2011-005>.
- , —, —, A. D. Fraser, and G. D. Williams, 2016: Sea ice production variability in Antarctic coastal polynyas. *J. Geophys. Res. Oceans*, **121**, 2967–2979, <https://doi.org/10.1002/2015JC011537>.
- Todd, A., and Coauthors, 2020: Ocean-only FAFMIP: Understanding regional patterns of ocean heat content and dynamic sea level change. *J. Adv. Model. Earth Syst.*, **12**, e2019MS002027, <https://doi.org/10.1029/2019MS002027>.
- Tsujino, H., and Coauthors, 2018: JRA-55 based surface dataset for driving ocean–sea-ice models (JRA55-do). *Ocean Modell.*, **130**, 79–139, <https://doi.org/10.1016/j.ocemod.2018.07.002>.
- Valcke, S., T. Craig, and L. Coquart, 2015: OASIS3-MCT user guide. CERFACS Tech. Rep., 54 pp., <http://www.cerfacs.fr/globc/publication/technicalreport/2015/OASIS3-UserGuide.pdf>.
- Xie, P., and G. K. Vallis, 2012: The passive and active nature of ocean heat uptake in idealized climate change experiments. *Climate Dyn.*, **38**, 667–684, <https://doi.org/10.1007/s00382-011-1063-8>.
- Zhang, L., T. L. Delworth, W. Cooke, and X. Yang, 2019: Natural variability of Southern Ocean convection as a driver of observed climate trends. *Nat. Climate Change*, **9**, 59–65, <https://doi.org/10.1038/s41558-018-0350-3>.
- Zika, J. D., N. Skliris, A. Blaker, R. Marsh, A. J. G. Nurser, and S. Josey, 2018: Improved estimates of water cycle change from ocean salinity: The key role of ocean warming. *Environ. Res. Lett.*, **13**, 074036, <https://doi.org/10.1088/1748-9326/aace42>.
- Zwally, H. J., and P. Gloersen, 1977: Passive microwave images of the polar regions and research applications. *Polar Rec.*, **18**, 431–450, <https://doi.org/10.1017/S0032247400000930>.
- Zweng, M., and Coauthors, 2018: *Salinity*. Vol. 2, *World Ocean Atlas 2018*, NOAA Atlas NESDIS 82, 50 pp.